

DOUBLE COMPACT OBJECTS I: THE SIGNIFICANCE OF THE COMMON ENVELOPE ON MERGER RATES

MICHAŁ DOMINI¹, KRZYSZTOF BELCZYŃSKI^{1,2}, CHRISTOPHER FRYER³, DANIEL E. HOLZ^{4,5}, EMANUELE BERTI^{6,7}, TOMASZ BULIK¹, ILYA MANDEL⁸, RICHARD O’SHAUGHNESSY⁹,

¹ Astronomical Observatory, University of Warsaw, Al. Ujazdowskie 4, 00-478 Warsaw, Poland

² Center for Gravitational Wave Astronomy, University of Texas at Brownsville, Brownsville, TX 78520

³ CCS-2, MSD409, Los Alamos National Laboratory, Los Alamos, NM 87545

⁴ Enrico Fermi Institute, Department of Physics, and Kavli Institute for Cosmological Physics
University of Chicago, Chicago, IL 60637

⁵ Theoretical Division, Los Alamos National Laboratory, Los Alamos, NM 87545

⁶ Department of Physics and Astronomy, The University of Mississippi, University, MS 38677, USA

⁷ California Institute of Technology, Pasadena, CA 91109, USA

⁸ School of Physics and Astronomy, University of Birmingham, Edgbaston, Birmingham, B15 2TT, UK

⁹ Center for Gravitation and Cosmology, University of Wisconsin-Milwaukee, Milwaukee, WI 53211, USA

Draft version April 11, 2019

ABSTRACT

The development of gravitational wave observatories (Advanced LIGO/Virgo, Einstein Telescope) is proceeding apace, and the direct detection of gravitational waves should be imminent. The last decade of observational and theoretical developments in stellar and binary evolution provides an opportunity to incorporate major improvements to the predictions from population synthesis models. We update the **StarTrack** code, and compute the rates for NS-NS, BH-NS, and BH-BH mergers. Among the most important revisions in the formation and evolution of double compact binaries are: updated wind mass loss rates (allowing for stellar mass black holes up to $80 M_{\odot}$), a realistic treatment of the common envelope phase (a process that can affect merger rates by 2–3 orders of magnitude), and a qualitatively new neutron star/black hole mass distribution (consistent with the observed “mass gap”). We present a parameter study with these major physical updates included, focusing on the most important factors that set the double compact object merger rates. A few of our more interesting findings include: *(i)* The binding energy of the envelope plays a pivotal role in determining whether a binary merges within a Hubble time, and our results depend sensitively on the model describing this. *(ii)* Our description of natal kicks from supernovae plays an important role, especially for the formation of BH-BH systems. *(iii)* The masses of BH-BH systems can be substantially increased in the case of low metallicities or weak winds. *(iv)* Certain combinations of parameters underpredict the Galactic NS-NS merger rate, and can be ruled out. *(v)* Models incorporating delayed supernovae do not agree with the observed NS/BH “mass gap”, in accordance with our previous work. And, finally, *(vi)* We find enhanced rates for BH-BH mergers as compared to previous estimates, with an expectation of ~ 100 such mergers per year in Advanced LIGO/Virgo detectors (although this rate is sensitive to the details of underlying models, such as the natal kick distribution). This is the first in a series of three papers. The second paper will study the merger rates of double compact objects as a function of cosmological redshift, star formation rate, and metallicity. In the third paper we will present the detection rates for future gravitational wave observatories, using up-to-date signal waveforms and sensitivity curves.

Subject headings: common envelope, supernova, black hole, neutron star

1. INTRODUCTION

We investigate the evolution of binary systems that leads to the formation of close double compact objects (DCOs) merging within a Hubble time: double neutron star (NS-NS), black hole–neutron star (BH-NS), and double black hole (BH-BH) systems. Only isolated evolution (i.e., in field populations) is considered. Several different groups have provided similar estimates in the past decade (Nelemans et al., 2001; Voss & Tauris, 2003; Dewi & Pols, 2003; Nutzman et al., 2004; Pfahl et al., 2005), and exploration of the relevant physical processes and rate estimates were obtained with the **StarTrack** population synthesis code (Belczynski et al., 2002, 2004, 2006, 2007, 2008, 2010a,b, 2011a; O’Shaughnessy et al., 2005a,b,c). In this paper we revisit these rate estimates, incorporating recent improvements to the input physics within the **StarTrack** code. Similar rate estimates performed for dense pop-

ulations in which dynamical interactions between stars are important (i.e., globular clusters) have been presented elsewhere (Gültekin et al., 2004; O’Leary et al., 2006; Grindlay et al., 2006; Sadowski et al., 2008; Ivanova et al., 2008; Downing et al., 2010; Miller & Lauburg, 2009).

To describe the formation of a double compact object one needs to know the history of both progenitors, as well as the interactions between them. However, the uncertainties associated with a number of evolutionary processes inhibit an accurate description. Among the most important unknowns are the details of the common envelope (CE) phase, the unknown maximum mass of the NS, the physics of the supernova explosions that form compact objects, and the wind mass loss rates of their progenitors. In this paper we approach the problem by calculating and investigating a suite of population synthesis models. The uncertainties are assessed by altering the parameters and input

physics within defined limits. This allows us to “bracket” our ignorance of the physical processes that are crucial for understanding double compact object formation.

In this paper we investigate the physics associated with the CE phase, focusing on the binding energy parameter, λ , and the structure of the donor star. We introduce a new treatment of the NS/BH formation processes in core collapse supernovae, and assess the role of natal kicks, the maximum NS mass, and wind mass loss on the rates. To show the basic dependence of our results on metallicity, we consider two fiducial stellar populations: $Z = Z_{\odot}$ and $Z = 0.1 Z_{\odot}$. Our main results are presented in Fig. 19 and 20. A broader metallicity study will be presented in paper II of this series, with inclusion of the cosmic star formation history, and a calculation of the dependence of rates on redshift. Paper III will examine the detection prognosis with advanced gravitational telescopes (e.g. Advanced LIGO/Virgo, Einstein Telescope), incorporating the latest gravitational waveforms and sensitivity curves for the various instruments.

In order to make the results of our research easily accessible to the community, we have provided an on-line **Synthetic Universe** database, available at www.syntheticuniverse.org. At present this contains detailed information on the population synthesis models in this paper. In addition, a number of physical parameters and their distributions that are not discussed here in detail (e.g., initial binary parameters, component masses, mass ratios, evolutionary tracks) are also provided, for those who might want to include them in their own research. We intend this database to act as an extension to our three papers, functioning as a repository of the full spectrum of our double compact object populations. The “Synthetic Universe” site will be updated in real time as new physical models are calculated, and will respond to requests from the scientific community. Eventually, the **Synthetic Universe** will include various objects in addition to double compact object binaries, for example stellar populations with white dwarfs (e.g., supernovae Ia progenitors; low frequency gravitational wave sources; cataclysmic variables) and various types of X-ray binaries (e.g., persistent and transient sources; high- and low-mass X-ray binaries in Galactic and extra-galactic environments).

In the next section we describe recent physical developments addressing the CE events, the wind mass loss rates from massive stars, supernovae explosions and compact object formation, incorporated into the **StarTrack** code. Section 3 contains a general description of the most important physical parameters used in our population synthesis, while in Section 4 we present the models used in this study, and our results. We summarize and conclude in Section 5.

2. STARTRACK IMPROVEMENTS

2.1. The StarTrack code

We have used the population synthesis code **StarTrack** to calculate the numbers and properties of DCOs. The full description of the code can be found in Belczynski et al. (2002, 2008). The code utilizes a set of stellar models (Hurley et al. (2000); slightly modified from its original version) that allow for the evolution of stars at different metallicities. The model for compact object formation adopted in the code has been significantly revised;

changes are described in Section 2.4. During core collapse, fallback and direct BH formation is now accounted for (Fryer & Kalogera, 2001) and the newly born objects receive natal kicks (Hobbs et al., 2005). The formation of low mass NSs through electron capture supernovae is also accounted for (e.g., Podsiadlowski et al. (2004)). Binary interactions are treated in detail, and the various physical processes have been calibrated using either results of detailed evolutionary calculations (e.g., Wellstein & Langer (1999) for mass transfer sequences), or specific sets of observations (e.g., Levine et al. (2000) for tidal interactions).

In the following sections we describe the major updates to the code that are relevant for the formation of BHs and NSs. These crucial improvements are based on advances in stellar evolution physics in the last decade. Included are revised rates for wind mass loss for massive stars that now allow for the formation of BHs with masses observed in the Milky Way and other galaxies (see Section 2.2). Another improvement relates to the CE coefficient, λ , describing the binding energy of the envelope. It is now dependent upon the parameters (mass, radius, etc.) and the evolutionary stage of the donor. This is a major improvement when compared to most previous studies, where λ was considered constant throughout the evolution of the donor (Section 2.3). The third major update regards the core collapse/supernova explosions, and the resulting model for compact object formation. We introduce two convection-enhanced, neutrino driven supernova engines (based on Rayleigh-Taylor and Standing Accretion Shock instabilities) into our population synthesis code. This addition allows us to account for the dearth of Galactic compact objects within the mass range 2–5 M_{\odot} (the so called “mass gap” (Section 2.4)).

2.2. Stellar winds

The **StarTrack** code was recently updated with new wind mass loss rates (described in detail in Belczynski et al. (2010a)). One of the major changes was the implementation of mass loss for O/B stars based on Vink et al. (2001), followed by new winds for Wolf-Rayet stars (Hamann & Koesterke, 1998; Vink & de Koter, 2005). Furthermore, the Luminous Blue Variable winds (based on Humphreys & Davidson (1994)) were calibrated so as to allow for the formation of BHs with masses up to 15 M_{\odot} in a solar metallicity environment. This was done in order to account for the observed masses of known BHs in the Milky Way (e.g. Orosz et al. (2011)). The most important consequence of these updates is the possibility of the formation of BHs with masses up to 30 M_{\odot} in sub-solar metallicity environments ($Z = 0.3Z_{\odot}$), which corresponds to the observed mass of the most massive known stellar-mass BH in the IC10 X-1 binary (Prestwich et al., 2007; Silverman & Filippenko, 2008). These revisions also result in the formation of BHs with masses up to 80 M_{\odot} in a low metallicity ($Z = 0.01Z_{\odot}$) environment.

2.3. Common envelope updates

We begin with an expression describing the energy balance of the CE (Webbink, 1984):

$$\alpha_{\text{CE}} \left(\frac{GM_{\text{don,f}}M_{\text{acc}}}{2A_{\text{f}}} - \frac{GM_{\text{don,i}}M_{\text{acc}}}{2A_{\text{i}}} \right) = \frac{GM_{\text{don,i}}M_{\text{don,env}}}{\lambda R_{\text{don,lob}}}. \quad (1)$$

Here, $R_{\text{don,lob}}$ is the Roche lobe radius of the donor at the onset of Roche lobe overflow (RLOF), A is the binary separation, $M_{\text{don,env}}$ is the mass of the ejected envelope, and M_{don} and M_{acc} are the masses of the donor and accretor, respectively. Indices i and f stand for initial and final parameters, respectively. The parameter α_{CE} describes the efficiency of the transfer of orbital energy into unbinding the envelope. If there is sufficient orbital energy to unbind the envelope the binary may survive the CE phase, otherwise the component merger and the formation of a peculiar single object is assumed (an example: if the accretor is a compact object then in the outcome of the CE a star harbouring a NS/BH may form). The value of α_{CE} has been set to 1 throughout this study. The range of values for the product $\alpha_{\text{CE}}\lambda$ may therefore be covered by λ alone. The parameter λ describes the binding energy of the envelope, and is defined as:

$$E_{\text{bind}} = -\frac{GM_{\text{don}}M_{\text{don,env}}}{\lambda R}, \quad (2)$$

where R is the radius of the donor, which becomes equal to the Roche lobe radius of the donor at the onset of the CE. The most significant changes of binding energy are usually associated with radial expansion or contraction of a star. Additionally, the mass loss/gain may alter the binding energy. Generally, as the envelope of the star expands it becomes less dense and so its binding energy decreases, while a contraction of the envelope leads to an increase in the binding energy. The parameter λ is a function of binding energy, radius, and mass (Eq. 2). For example, λ will decrease if the radius expands faster than the binding energy decreases, which is the case for stars on the Hertzsprung gap (HG) stars (Fig. 1–4). If the radial expansion of a star remains moderate, λ may increase as it happens on the Red Giant Branch (RGB) and Asymptotic Giant Branch (AGB) (see Fig. 1). For the most massive stars (initial mass above $\sim 20 M_{\odot}$) the mass loss becomes a significant factor, and the changes in density profile, radius, and binding energy result in an almost constant λ during later evolutionary stages (see Fig. 2–4).

Most importantly, Eq. 2 implies that given the mass, radius, and evolutionary state (i.e. the envelope size) of a donor, a change of λ will change the binding energy of its envelope. For example, the binding energy of the envelope of a star with $\lambda = 0.1$ will be larger by an order of magnitude as compared to an identical star with $\lambda = 1$. During the CE phase, orbital energy is used to eject the envelope. Therefore, a binary will have much more difficulty ejecting the tightly bound envelope of a donor with $\lambda = 0.1$, as compared with one with $\lambda = 1$.

The consequences for the formation of double compact objects are twofold. If λ has a low value, and the stars have insufficient separation (orbital energy), they will merge during the CE phase. This terminates further binary evolution and prevents the formation of a DCO. If, on the other hand, λ has a high value, it is most likely that a given system will eject the CE with a small resulting decrease in orbital separation. Binaries (later becoming DCOs) retaining a wide enough separation after the CE event may not be able to merge within a Hubble time. Such DCOs become uninteresting from the gravitational wave detection perspective. Also, a supernova explosion occurring in

a binary that maintains a wide orbital separation tends to disrupt the system.

2.3.1. Hertzsprung gap donors

The outcome of the CE phase depends strongly on the evolutionary stage of the donor, as first discussed in Belczynski et al. (2007). Even before considering the energy balance, it is critical to incorporate an understanding of the core-envelope structure of the star. For example, Main Sequence (MS) stars do not have clear core-envelope division, as the helium core is still in the process of being developed. Stars on the HG similarly lack a clear entropy jump associated with the core-envelope structure (Ivanova & Taam, 2004), although when in the evolution such a division appears (late HG or post HG?) remains unclear. In the case of a CE initiated by a MS or HG donor, therefore, the orbital energy is transferred into the entire star rather than just the envelope. This makes the ejection of the envelope difficult, and for MS stars we assume that this will always result in a merger. However, in the case of HG we extend the analysis by considering two possibilities. One is to ignore the core-envelope boundary issue, and proceed with the calculation of the energy balance (submodel A). The second is to adopt a pessimistic approach (submodel B) in which each CE with a HG donor leads (independent of energy balance) to a merger. Both submodels are calculated for each evolutionary model in this study. Massive stars, beyond HG, that enter the core helium burning already possess well-defined core-envelope structure and require only the energy balance calculation. Exceptions are the Helium MS and Helium HG stars, which have an analogous structure to their hydrogen counterparts, and are treated as such.

2.3.2. New calculation of the λ parameter

A physical estimate of λ was recently presented by two groups: Xu & Li (2010) and Loveridge et al. (2011). We adopt the expressions from the former group in the **StarTrack** code, although both calculations yield similar results for NS/BH progenitors. The new λ values cover CE events, and depend on the evolutionary stage of the donor, its mass at Zero Age Main Sequence (ZAMS) and the mass of its envelope, and its radius. In addition, all of these quantities can depend on a wide range of metallicities ($Z = 10^{-4}$ –0.03). This represents a significant improvement in the physics of the formation of DCOs, as most previous studies treated λ as constant (usually $\lambda = 1$) throughout the evolution of a star. In the new approach the authors calculate two values of λ from detailed stellar models: in the first they treat the binding energy of the donor’s envelope as consisting only of its gravitational energy, while in the second the binding energy is decreased by the full internal energy of the envelope. Since neither of these extremes is plausible (Xu & Li, 2010), we choose our λ to be the average of the two. In the case of stars with masses leading to the formation of BHs we find that $\lambda \lesssim 1$ (see Fig. 3,4). We find higher values for typical NS progenitors, and especially in the late evolutionary stages we have $\lambda \gtrsim 1$ (see Fig. 1). Since the group that developed this procedure is affiliated with Nanjing University, we label this approach as the *Nanjing* λ . We have additionally requested that the authors compute a few extra

models for massive stars, as these are particularly relevant to our study. Xu & Li (2010) presents models up to $M_{\text{zams}} = 20 M_{\odot}$, and we have now obtained models up to $M_{\text{zams}} = 100 M_{\odot}$. We then extrapolate these to our entire mass range (up to $M_{\text{zams}} = 150 M_{\odot}$). For stars with $M_{\text{zams}} > 100 M_{\odot}$ we use the fitting function calculated for $M_{\text{zams}} = 100 M_{\odot}$, but input the higher mass when necessary.

2.4. Compact object formation

To evolve a star from ZAMS toward its eventual supernova (SN) with the *StarTrack* code, we use the (slightly modified; see Belczynski et al. (2002)) procedure presented in Hurley et al. (2000), with updated wind mass loss rates as described in Section 2.2. The mass of the compact object is calculated from the properties of the pre-supernova star, and the type (whether it is a NS or a BH) is set solely by its mass.

We use a recent study by Fryer et al. (2011) to describe the SN explosion and the resulting compact object formation. Our models allow for a successful explosion without the need for the artificial injection of energy into the exploding star. This is a major update of the input physics used in the population synthesis of massive binaries. Previous studies at best used significantly outdated supernova models, if they used any at all. We have introduced two alternative supernova models into our code: “Delayed” and “Rapid”. Both are core-collapse scenarios, and they share the same convection-enhanced neutrino-driven explosion mechanism. The main factor that differentiates the two models is the type of instability which causes the macroscopic flows of matter (similar to convection) that eventually lead to the ejection of the infalling matter. The Delayed model is sourced from the standing accretion shock instability (SASI), and can produce an explosion as late as 1 s after bounce, while the Rapid model starts from the Rayleigh-Taylor instability and occurs within the first 0.1–0.2 s. In the Rapid scenario we either end up with a very strong (high velocity kick) supernova in the case of a low mass star ($M_{\text{zams}} \lesssim 25 M_{\odot}$), and produce a NS, or the supernova fails, and there is direct collapse to a massive BH. In the Delayed case the entire spectrum of explosion energies is allowed, and this results in a wide range of compact object masses, from NSs to light BHs to massive BHs. The formulae describing the two supernova engines adopted in *StarTrack* are provided in Fryer et al. (2011) (Eqs. 15–20).

We also allow for the formation of NSs through Electron Capture Supernovae (ECS, Miyaji et al. (1980)). These are weak supernovae (no natal kick assumed) occurring for the lowest mass stars ($M_{\text{zams}} \sim 7 M_{\odot}$), and they end up forming NSs.

3. MODELING

The physics underlying the formation of double compact objects is uncertain, notably due to modelling challenges of the supernova and CE phases. Core collapse, usually (but not always) followed by a supernova explosion, forms a compact object. The mass and the type of compact object is determined by the details of the event. Additionally, supernova asymmetry via mass loss and/or a natal kick may disrupt a binary, depleting the population of

double compact objects. At the same time, for some binaries a natal kick of the right amplitude and direction may produce a prematurely coalescing DCO. The CE phase is present in all formation scenarios, for all types of close double compact objects. It is the primary mechanism for bringing initially widely-separated binaries into close orbits, thereby allowing them to coalesce within a Hubble time.

To explore the uncertainties associated with our models we calculate a suite of population synthesis results, investigating a range of factors which have the largest impact on the rates and physical properties of DCOs. As a reference we use the standard model introduced in Section 4.1, that resembles input physics described in detail in Belczynski et al. (2008), with some important additions and modifications. The subsequent models are variations on this standard model, each exploring a single parameter connected to either the core collapse/supernova explosion or CE phases. Despite the fact that we now have physically motivated values for λ , we also explore models in which λ is constant, with the specific value set over a wide range. The range is chosen to be such as to encompass all plausible values allowed by detailed physical calculation of the *Nanjing* results (Xu & Li, 2010). Variations 1–4 employ $\lambda = 0.01, 0.1, 1, \text{ and } 10$, respectively (see Table 1).

To delineate between a NS and a BH we need to adopt a value for the maximum NS mass. Theoretical studies of the equation of state allow values in the range 1.5–3.0 M_{\odot} (Lattimer & Prakash, 2010). Observations yield a narrower range, with the most massive NSs reaching 2 M_{\odot} (Demorest et al., 2010). Statistical analyses of the measured BH masses indicate that the BH mass distribution is unlikely to extend below about 4.5 M_{\odot} (Bailyn et al., 1998; Özel et al., 2010; Farr et al., 2011), which leaves a significant range with no compact objects. This might argue for a higher upper limit on the NS mass (or even potentially a lower limit on the BH mass?). Utilizing the theoretical and observational estimates, we vary the maximum NS mass from 3.0 M_{\odot} (Variation 5), through 2.5 M_{\odot} (Standard), and as low as 2.0 M_{\odot} (Variation 6).

In the standard model for natal kicks in core collapse supernovae we employ a Maxwellian kick distribution with $\sigma = 265 \text{ km s}^{-1}$, based on observed velocities of single Galactic pulsars (Hobbs et al., 2005). The magnitude of the kicks is modified by the amount of fallback during a SN as follows:

$$V_k = V_{\text{max}}(1 - f_{\text{fb}}), \quad (3)$$

where V_k is the final magnitude of the natal kick, V_{max} is the velocity drawn from a Maxwellian kick distribution, and f_{fb} is the fallback factor. The values of f_{fb} range between 0–1, with 0 indicating no fallback/full kick and 1 representing total fallback/no kick (in this case a “silent supernova”). This factor is calculated for both the Delayed and Rapid SN engines according to Fryer et al. (2011). For the electron capture supernovae the explosions are found to be symmetric (Dessart et al., 2006), and we assume no natal kick. However, the orbit is still modified due to the mass loss in the explosion. BHs that form through partial fall back are assumed to receive natal kicks that are drawn from the same distribution as for the NSs, but the value is decreased in proportion to the amount of fall back. In particular, the most massive BHs form via full fall back, which

leads to no natal kick and “silent” BH formation. This may be supported both theoretically (Fryer & Kalogera, 2001) and from observations (Mirabel & Rodrigues, 2003).

There seems to be some evidence that NSs that are found in binaries receive smaller natal kicks (e.g., Belczynski et al. (2010c); Wong et al. (2010); Bodaghee et al. (2011)), of the order of 100 km s^{-1} . Keeping the same Maxwellian distribution as in the standard model, we modify the magnitude of natal kicks of NSs and BHs to $\sigma = 132.5 \text{ km s}^{-1}$ (Variation 7).

Additionally, we calculate two models in which the BH kicks take on two extreme values. In one, newly formed BHs receive full natal kicks as, observed for single pulsars ($\sigma = 265 \text{ km s}^{-1}$) independent of the amount of fallback (Variation 8). In the other, no natal kicks are applied to BHs, independent of their mass or the amount of fallback (Variation 9).

As our standard model we select the Rapid supernova engine, since this supernova mechanism, combined with binary evolution, successfully reproduces the mass gap (Belczynski et al., 2011b) observed in Galactic X-ray binaries (Bailyn et al., 1998; Özel et al., 2010). On the other hand, the Delayed engine (Variation 10), as well as the routine previously implemented within **StarTrack** (Belczynski et al., 2002), generates a continuous spectrum of compact object masses.

Observational and theoretical developments have led to the discovery of a number of puzzling phenomena in the winds from massive stars. The two most prominent are the “weak wind problem” (e.g., Chlebowski & Garmany (1991); Kudritzki et al. (1991); Herrero et al. (2002)) and “wind clumping” (e.g., Osterbrock & Flather (1959); Markova et al. (2004); Repolust et al. (2004); Lépine & Moffat (2008)). The former is related to the fact that wind mass loss rates from late O and early B type stars might be ~ 1 – 2 orders of magnitude lower than theoretically predicted. The latter suggests that winds might be forming dense clumps rather than being distributed uniformly, which may lead to an overestimate of mass loss rates by a factor of $\lesssim 2$. Based on this we investigate the possibility that our wind mass loss rates are too high, and so we calculate a model (Variation 11) in which the rates are reduced by a factor of 2. This is done for all stars at all points in their nuclear evolution.

Table 1 lists all of our models, each with the relevant parameter to be varied as compared to our standard model (listed in the first row). Each model is calculated for two metallicity values: solar ($Z = Z_{\odot} = 0.02$) and 10% solar ($Z = 0.1 Z_{\odot} = 0.002$). Each model is further divided into submodel A (CE energy balance with HG donor) and submodel B (CE merger with HG donor) as discussed in Section 2.3.1. We end up with 45 distinctive models (11 variations for 2 metallicities and 2 CE submodels, on top of our standard model).

For each model we evolve 2×10^6 binaries (with one exception, see. Sec. 4.5), assuming that each component is created at the same time. Each binary system is initialized by four parameters which are assumed to be independent. These are: primary mass M_1 (initially more massive component), mass ratio $q = M_2/M_1$, where M_2 is the mass of the secondary component (initially less massive), the semi-

major axis a of the orbit, and the eccentricity e . The mass of the primary component is randomly chosen from the initial mass function adopted from Kroupa et al. (1993), and Kroupa & Weidner (2003),

$$\Psi(M_1) \propto \begin{cases} M_1^{-1.3} & 0.08 M_{\odot} \leq M_1 < 0.5 M_{\odot} \\ M_1^{-2.2} & 0.5 M_{\odot} \leq M_1 < 1.0 M_{\odot} \\ M_1^{-\alpha} & 1.0 M_{\odot} \leq M_1 < 150 M_{\odot}, \end{cases} \quad (4)$$

where $\alpha = 2.7$ is our standard choice for field populations. Stars are generated from within an initial mass range M_{min} – M_{max} , with the limits based on the targeted stellar population. For example, NS studies require evolution of single stars within the range 8–25 M_{\odot} , while for BHs the lower limit is 25 M_{\odot} . Binary evolution may broaden these ranges due to mass transfer episodes, and we therefore set the minimum mass of the primary to 5 M_{\odot} . We assume a flat mass ratio distribution, $\Phi(q) = 1$, over the range $q = 0$ – 1 , in agreement with recent observations (Kobulnicky & Fryer, 2007). Given a value of the primary mass and the mass ratio, we obtain the mass of the secondary from $M_2 = qM_1$. However, for the same reasons as for the primary, we don’t consider binaries where the mass of the secondary is below 3 M_{\odot} . The distribution of initial binary separations is assumed to be flat in $\log(a)$ (Abt, 1983), and so $\propto \frac{1}{a}$, with a ranging from values such that at ZAMS the primary fills no more than 50% of its Roche lobe to $10^5 R_{\odot}$. For the initial eccentricity we adopt a thermal equilibrium distribution (e.g., Heggie (1975); Duquennoy & Mayor (1991)) $\Xi(e) = 2e$, with e ranging from 0 to 1.

4. RESULTS

The double compact object merger rates for a synthetic galaxy resembling the Milky Way, but for two differing values of metallicity, are presented in Table 2 ($Z = Z_{\odot}$) and Table 3 ($Z = 0.1 Z_{\odot}$). The corresponding plots of the merger rates are shown in Figures 19 and 20. The physical properties of double compact objects for the standard model are presented in Figure 7 (chirp mass), Figure 8 (delay time), and Figure 9 (mass ratio). The distribution of chirp masses (Figures 10–13 (with corresponding Tables 6–9) and delay times (Figures 14–17) for all the models are presented. The delay time, t_{del} , is the sum of the time needed to form two compact objects from a ZAMS binary and the time for the two compact objects to coalesce due to the emission of gravitational radiation. For double compact objects the former evolutionary time interval ($\sim \text{Myr}$) is usually much shorter than the latter merger time ($\sim \text{Gyr}$), and the delay time is rather similar to the merger time. Additional models and DCO population properties are available on-line at www.syntheticuniverse.com.

For each model we calculate the Galactic merger rates. These are defined as the number of coalescences of DCOs per unit time occurring in a synthetic galaxy similar to the Milky Way (with age of 10 Gyr and a constant star formation rate (SFR) of $3.5 M_{\odot} \text{ yr}^{-1}$). In practice this is done by checking if the delay time of a DCO (with a random starting point between 0–10 Gyr) falls near the current galaxy age (10 Gyr). However, the amount of mass within the simulated binaries corresponds only to a part of the star forming mass of the galaxy. In order to extrapolate the simulated mass to that of the entire galaxy we em-

ploy the following procedure. First, the amount of mass contained within the simulated binary stellar population is estimated (the mass of the primary follows from Eq. 4, and the mass of the secondary follows from our assumed mass ratio distribution). Additionally, we assume a binary fraction of 50%, so that for each binary system there is one additional individual star. The mass of each of the individual stars is taken to be in the same range as for primary components in binaries. The acquired mass, M_{acq} , is then divided by the age of the synthetic galaxy t_{gal} (10 Gyr) in order to get a constant star formation rate corresponding to the simulated stellar mass ($0.073 M_{\odot} \text{ yr}^{-1}$). To match this SFR to the one of the synthetic galaxy SFR_{gal} ($3.5 M_{\odot} \text{ yr}^{-1}$) one needs a multiplication factor of 48 (f_{SFR}). The corresponding equation is:

$$f_{\text{SFR}} = \text{SFR}_{\text{gal}} \left(\frac{M_{\text{acq}}}{t_{\text{gal}}} \right)^{-1} \quad (5)$$

Therefore, to extrapolate our results to the entire mass in the synthetic Milky Way, we use each synthetic DCO binary 48 times. Each time the given binary is assigned a new starting time (from a uniform distribution), and if its coalescence time falls within 9–10 Gyr it is included in our results.

The typical range of the number of DCOs, N , generated in each simulation is ~ 1000 – 10000 for submodel A and ~ 10 – 100 for submodel B. Therefore the relative statistical error (\sqrt{N}/N) is at most $\sim 10\%$ – 30% where the ranges are given by the values in submodels A–B). The errors arising from uncertainties in various aspects of the single and binary star evolution can change the Galactic merger rates of DCOs by ~ 1 – 2 orders of magnitude (as shown in the next sections), making the statistical errors irrelevant.

In addition to the population of DCOs with delay times below 10 Gyr (the merging population), in each model we acquire another population occupying the domain above this time limit (the non-merging population). This population contains each type of DCO, and is available at www.syntheticuniverse.org.

4.1. Standard Model

At solar metallicity, the merger rates for a synthetic galaxy similar to the Milky Way are dominated by NS-NS systems (23.5 – 7.6 Myr^{-1} ; submodel A–B), with a smaller but still significant contribution from BH-BH systems (8.2 – 1.9 Myr^{-1}), and with a minor contribution from BH-NS systems to the overall DCO merger rate (1.6 – 0.2 Myr^{-1} ; see Table 2). Qualitatively these findings are consistent with previous results (Belczynski et al., 2002). The quantitative results, however, are quite different, due to the many improvements in the models over the intervening decade. Belczynski et al. (2002) found the following mean rates: NS-NS 53 Myr^{-1} , BH-BH 26 Myr^{-1} and BH-NS 8.1 Myr^{-1} . At sub-solar metallicity, the systems with BHs increase their relative contribution to the overall rates, and the merger rate is dominated by BH-BH systems (73.3 – 13.6 Myr^{-1}), with smaller contribution from NS-NS (8.1 – 2.5 Myr^{-1}) and BH-NS systems (3.4 – 2.3 Myr^{-1} ; see

Table 3). These results are qualitatively similar to our recent work on the dependence of merger rates on metallicity (Belczynski et al., 2010b). Again, quantitatively there are significant differences. Belczynski et al. (2010b) found the following rates: 84 – 6.1 Myr^{-1} (BH-BH), 41 – 3.3 Myr^{-1} (NS-NS) and 12 – 7.0 Myr^{-1} (BH-NS) for $Z = 0.1 Z_{\odot}$. These changes reflect the fact that since the previous study we have introduced physical λ values and observationally constrained SN models, which yields a new compact object mass spectrum.

A general division of these rates by DCO type may be understood in the following way. The initial mass function (IMF) falls steeply with mass, and delivers more NS than BH progenitors (by a factor ¹ of ~ 4). The supernova explosion is the major process that drastically affects the number of massive binaries, as the explosions tend to disrupt binaries. This is especially true in the case of NS progenitors, as these receive large natal kicks and as many as ~ 90 – 95% of potential binaries may end up disrupted after the first supernova explosion (e.g., Lorimer et al. (2004); Belczynski et al. (2010c)). Supernovae do not affect binaries with BHs as much because it is believed that most of the massive stars producing BHs do not experience large kicks at core collapse. What follows is that the rates for NS-NS and BH-BH mergers are not as separated as would be simply deduced from the IMF. The rates are also very sensitive to the details of the CE, and these are quite different for NS and BH progenitors (as discussed below). Additionally, the three types of double compact objects evolve along separate evolutionary channels (see Table 4). This qualitative picture can explain the calculated ratio of NS-NS to BH-BH merger rates (~ 3 – 4). The BH-NS merger rates are the smallest, as the majority of potential progenitor binaries have initially large mass ratios, and the first interaction of the two components leads to a CE phase and the inevitable merger. This happens because the massive envelope of the BH progenitor cannot be successfully dispersed by the much less massive NS progenitor. Note that none of the significant BH-NS formation channels starts with the CE phase, but instead the progenitors of these systems originate from a narrow mass range (mass ratio of the two components larger than $\sim \frac{1}{2}$ – $\frac{1}{3}$ allowing for the first interaction to be a stable RLOF (see Table 4).

At sub-solar metallicity other factors come into play and make BH-BH systems dominant in the overall merger rate. First, the smaller wind mass loss makes pre-SN progenitors of NSs slightly more massive (by $\sim 10\%$). Heavier NS progenitors tend to explode as core collapse supernovae (full kicks) rather than ECSe (no kicks, see Section 2.4). This means that for sub-solar metallicity more NSs are formed with disruptive natal kicks than for a solar environment. Additionally, smaller wind mass loss decreases the expansion of the separation between the components. This causes the progenitors of NS-NS systems, at sub-solar metallicities, to engage in a second CE (see Table 5) just after the first one. This increases the probability of a merger during evolution when compared with Z_{\odot} , hence the drop of merger rates of NS-NS systems from Z_{\odot} to $0.1 Z_{\odot}$. The merger rates for BH-BH systems increase for sub-solar metallicity, as low wind mass loss rates allow the

¹This factor is the ratio of the number of stars between 8–20 M_{\odot} (NS progenitors) to the number of stars between 20–150 M_{\odot} (BH progenitors) as calculated from the IMF (see Section 3).

progenitors to remain more massive during evolution. This in turn makes the pre-SN stars more massive and allows for larger amount of fallback. Increased fallback reduces the magnitude of the natal kicks (see Eq. 3) to almost none or none at all (direct collapse into a BH) and makes the SN significantly less disruptive, as explained in detail by Belczynski et al. (2010b).

The formation of BH-NS binaries is determined by the properties of the progenitors of both compact object types. Therefore, the behaviour of these systems may be considered as a combination of effects noted in the formation of BH-BH and NS-NS systems.

In Figures 5, 6, 7, 8 and 9 we present the distributions of DCO progenitor ZAMS masses, DCO masses, chirp masses, delay times and DCO mass ratios for the standard model. For purposes of illustration, the distribution of progenitor and remnant masses are given for submodel A, $Z = Z_{\odot}$ only. Additional plots are available at www.syntheticuniverse.org.

In the distribution of progenitor ZAMS masses (Fig. 5) one can clearly see that binary evolution blurs the limits for ZAMS mass of the star for the formation of NS/BH. For NS-NS progenitors (top panel), the masses of the primary components (up to $\sim 30 M_{\odot}$) exceed the typical upper limit for the formation of a NS for single stars ($\sim 20 M_{\odot}$, also lower limit for the formation of a BH). Under favourable circumstances, binary evolution may push this limit even further, up to $100 M_{\odot}$ (e.g., Wellstein et al. (2001); Belczynski & Taam (2008)). Note that for BH-NS systems (middle panel), a high progenitor mass does not necessarily imply that it will form a BH. During their evolution, progenitors of BH-NS systems may undergo a mass ratio reversal (due to mass transfer events) so the primary component (initially more massive) may become a NS (as seen on the middle panel of Fig. 6). For BH-BH progenitors the lowest mass of the primary component is $\sim 45 M_{\odot}$, and the lowest mass of the secondary is $\sim 25 M_{\odot}$. Also, progenitor stars of BH-BH systems have a wide mass distribution (ranging up to $150 M_{\odot}$). However, the masses peak at $\sim 55 M_{\odot}$ for the primary component and $\sim 40 M_{\odot}$ for the secondary.

The distribution of masses of DCO remnants (Fig. 6) clearly shows the gap between the upper mass achievable by NSs ($2 M_{\odot}$, despite allowing for the formation of NSs with mass up to $2.5 M_{\odot}$) and the lower mass of BHs ($\sim 5 M_{\odot}$). This is due to the implementation of the Rapid supernova engine, which is the first to successfully reproduce this “mass gap” (for details see Section 2.4). Additionally, for BH-NS binaries some remnants formed out of the initially less massive star in the binary fall within the BH mass regime while some primary components (initially more massive) may end up as NSs. This is due to the aforementioned mass ratio reversal. Despite a wide range of BH-BH progenitor masses, the component masses of remnant systems are mostly clustering around $5\text{--}9 M_{\odot}$. Such a drastic reduction in mass range comes from the significant wind mass loss for massive BH progenitors and mass ejection in CE events. Both factors usually reduce the masses of the whole progenitor stars to the masses of their cores, for which the mass range is narrow.

To calculate the chirp mass M_{chirp} of a DCO we use the

following formula:

$$M_{\text{chirp}} = (M_1 M_2)^{\frac{3}{5}} (M_1 + M_2)^{-\frac{1}{5}}, \quad (6)$$

where M_i are the masses of the components. The most notable aspect of the chirp mass distributions (Fig. 7) is the maximum value for BH-BH systems ($\sim 30 M_{\odot}$), for submodel A, $0.1 Z_{\odot}$. As metallicity decreases from solar to sub-solar, so do the wind mass loss rates. This allows for the formation of more massive BHs. For submodel B, $Z = 0.1 Z_{\odot}$ the maximum value is lower ($18 M_{\odot}$) than for submodel A for the same metallicity. In submodel A the most massive progenitors of BHs experience significant expansion during evolution leading to the CE events with a HG donor, rather than a donor beyond the HG which is more likely for lower mass progenitors. Submodel B does not allow for the survival of HG donors during a CE (see Section 2.3.1) and the most massive BHs disappear. The average chirp masses for $Z = Z_{\odot}$ are the same for both submodels: 1.05 for NS-NS, $3.2 M_{\odot}$ for BH-NS, and $6.7 M_{\odot}$ for BH-BH systems. For $0.1 Z_{\odot}$ the average chirp masses are: $1.1\text{--}1.1 M_{\odot}$ (submodel A–B) for NS-NS, $3.2\text{--}3.1 M_{\odot}$ for BH-NS, and $13.2\text{--}9.7 M_{\odot}$ for BH-BH systems.

The delay time distributions (Fig. 8) are proportional to t_{del}^{-1} . The average delay time for systems merging within 10 Gyr at Z_{\odot} is: $1.1\text{--}1.5$ Gyr (submodel A–B) for NS-NS, $1.7\text{--}1.7$ Gyr for BH-NS, and $1.0\text{--}2.5$ Gyr for BH-BH systems. For sub-solar metallicity the average is: $1.0\text{--}2.3$ Gyr for NS-NS, $1.5\text{--}1.5$ Gyr for BH-NS, and $1.0\text{--}1.4$ Gyr for BH-BH systems.

The delay times for submodel B are in general higher than for submodel A. This is a direct result of our assumption on the outcome of the CE phase with HG donor. Binary populations are identical in submodel A and B until a CE event. If the separation is relatively small, the CE may be initiated early on in the evolution, specifically by a HG donor. The survival of such an event may lead to the formation of a close binary in submodel A. In submodel B CEs with this type of donor are always considered a merger (see Section 2.3.1). Binaries with separation large enough to prevent the rapidly expanding HG star from overflowing its Roche lobe will initiate the CE in later stages of evolution. This scenario meets the criteria of A and B submodels and allows the binaries to be accounted in both (in terms of forming merging DCOs). Submodel B, therefore, favours binaries with larger separations, which translate into larger merger times.

Additionally, the delay times decrease with metallicity. This comes from the fact that for sub-solar environments stars lose less mass in winds and therefore, form more massive remnants. The more massive the components of a DCO, the less time it takes for a system to merge. A secondary effect of the reduced wind mass loss rates for $Z < Z_{\odot}$ on the delay times is the smaller expansion of the separation during evolution as a smaller amount of mass is removed from the system.

The distribution of mass ratios q is similar for both submodels and both metallicities. NS-NS systems group around $q = 0.9$ as the NS masses found in our models are on average similar in each formed DCO system ($\sim 1.1\text{--}1.4 M_{\odot}$; see Fig. 6). BH-NS systems group around small mass ratio values ($q = 0.2$), which means a large difference in mass between both remnant compact objects. This fol-

lows from the fact that the typical NS mass is $1.3 M_{\odot}$ and the typical BH mass is found at $5\text{--}9 M_{\odot}$ (see Fig. 6). BH-BH systems have the widest range of q , and typically our simulations show mass ratios in the range $0.4\text{--}1.0$ with increasing probability toward $q = 1$. This simply reflects the fact that BH progenitors come from a wide range of masses, and that binaries with similar masses more readily survive binary interactions (mass transfers and supernovae explosions).

4.2. Variation 1

This is the first of four variations addressing the CE binding energy parameter, λ . In this model we fix $\lambda = 0.01$. It is found that in this evolutionary variation all merger rates significantly decrease as compared to the standard model (see Table 2 and 3). For solar metallicity the Galactic merger rates are dominated by BH-BH systems (1.1 Myr^{-1} for both submodels), followed by NS-NS (0.4 Myr^{-1} for both submodels), and BH-NS systems (0.002 Myr^{-1} , also for submodels A and B). For $0.1 Z_{\odot}$ the rates for BH-BH systems are $12.5\text{--}8.1 \text{ Myr}^{-1}$ (submodel A–B), 0.06 Myr^{-1} for NS-NS systems (for both submodels), and 0.03 Myr^{-1} for BH-NS systems (also for both submodels). The behaviour of the population of double compact objects in this model can be understood as follows. We have chosen λ to have a very low value, which translates into a very high binding energy of the CE (see Eq. 2). This binding is so strong that most of the binaries experience a merger during the first CE phase in their evolutionary history. This terminates the evolution of the binary and prevents the formation of a DCO. The least affected are BH-BH systems, since the fixed λ value used in this variation is comparable to (although lower than) the *Nanjing* λ (see Fig. 3,4) of the typical BH progenitor.

In earlier stages, such as on the Hertzsprung gap, the values are higher (*Nanjing* $\lambda \approx 0.1\text{--}0.2$; see Fig. 3). This means that in this fixed λ scenario the value of the binding energy of the CE of a HG donor is an order of magnitude larger than for the standard (more physical) model. Therefore, many CE events with a HG donor end in a merger, as the reservoir of the orbital energy is insufficient to eject the envelope. The surviving binaries are the ones in which the CE was initiated by a CHeB donor and/or that have very massive accretors and therefore a large orbital energy reservoir. Submodel B does not allow for CE events with a HG donor. In effect, the very small λ (very large binding energy) adopted in submodel A also prevents binaries from surviving a CE event with a HG donor, just as in submodel B. As a result, the binary populations formed in the two submodels are very similar.

For $Z = Z_{\odot}$ the average chirp mass for NS-NS systems is $1.1 M_{\odot}$, $3.2 M_{\odot}$ for BH-NS, and $6.5 M_{\odot}$ for BH-BH systems (for both submodels). In both submodels the distributions of chirp masses in the standard model and V1 are similar. The slight differences come from the fact that the population of merging DCOs in V1 is composed of binaries that would form the non-merging population in the standard model. For $Z = 0.1 Z_{\odot}$ the corresponding values are $1.1 M_{\odot}$ for NS-NS and $3.6 M_{\odot}$ for BH-NS systems (for both submodels). In the case of BH-BH systems the average chirp mass is $20.0 M_{\odot}$ for submodel A and $16.1 M_{\odot}$ for submodel B. For $Z = 0.1 Z_{\odot}$, submodel A, the distribution of BH-BH chirp masses is flatter in V1 than for

the standard model. Specifically, there are fewer low chirp mass systems in V1 than for the standard model. There are two mechanisms determining this outcome. The first is the increased number of mergers during the CE in this variation, which reduces the overall number of DCOs. The second is the fact that less massive BH-BH systems have relatively light progenitors. These binaries have smaller chances of ejecting such a strongly bound CE due to a smaller orbital energy reservoir, and merge in the process.

Since the populations in submodels A and B are similar, we find similar distributions of chirp masses and delay times. For $Z = Z_{\odot}$ the average chirp mass for NS-NS systems is $1.09 M_{\odot}$, $3.2 M_{\odot}$ for BH-NS, and $6.5 M_{\odot}$ for BH-BH systems. For $Z = 0.1 Z_{\odot}$ the values are $1.11 M_{\odot}$ for NS-NS, $3.6 M_{\odot}$ for BH-NS systems for both submodels, while for the BH-BH systems the average chirp mass is $20.0 M_{\odot}$ for submodel A and $16.1 M_{\odot}$ for submodel B. The components of these BH-BH systems belong to the most massive compact objects, and this results in the high cutoff point of the chirp mass distribution in submodel B for $0.1 Z_{\odot}$ ($\sim 30 M_{\odot}$), when compared to other variations. Due to the very low λ in V1, only very wide progenitor binaries can survive a CE phase. These binaries would form non-merging ($t_{\text{del}} > 10 \text{ Gyr}$) BH-BH systems in the standard model. Since the progenitor binaries are very wide, the CE is typically initiated when the donor expands significantly. This happens at late evolutionary stages and/or for very massive donors; therefore, the donor in most cases has already evolved past the HG and is in the CHeB phase. As most donors are CHeB stars, both submodels produce very similar populations. Furthermore, since many progenitors are very massive stars, they produce very massive BH-BH systems in both submodels.

The average delay times for Z_{\odot} are $\sim 52 \text{ Myr}$ for NS-NS, $\sim 1.7 \text{ Gyr}$ for BH-NS, and $\sim 1.5 \text{ Gyr}$ for BH-BH systems. For $0.1 Z_{\odot}$ these are $\sim 82 \text{ Myr}$ for NS-NS, $\sim 0.8 \text{ Gyr}$ for BH-NS for both submodels. For BH-BH systems we find average delay $\sim 480 \text{ Myr}$ for submodel A and $\sim 680 \text{ Myr}$ for submodel B. The short delay times for NS-NS systems is a direct consequence of the very low value of λ . The high binding energy of the envelope following from this causes significant orbital energy dissipation. This prevents the formation of NS-NS systems with delay times over 300 Myr (see Fig. 14–17).

Due to the severe reduction in the total number of systems in this model, the least populated group, BH-NS systems, is subject to larger statistics errors. For example, for solar metallicity we find only 1 merging BH-NS system in the V1 model. However, as we will see below, this model can be excluded based on observations of known NS-NS Galactic systems, and therefore we do not follow up with additional computations.

4.3. Variation 2

In this model we fix $\lambda = 0.1$. The rates for solar metallicity, for the DCOs are: $11.8\text{--}1.1 \text{ Myr}^{-1}$ for NS-NS, $2.4\text{--}0.08 \text{ Myr}^{-1}$ for BH-NS, and $15.3\text{--}0.4 \text{ Myr}^{-1}$ for BH-BH systems (submodel A–B). For sub-solar metallicity NS-NS ($65.9\text{--}6.9 \text{ Myr}^{-1}$) and BH-BH systems ($56.7\text{--}16.1 \text{ Myr}^{-1}$) strongly dominate the DCO merger rate, with relatively insignificant rates for BH-NS systems ($0.5\text{--}0.4 \text{ Myr}^{-1}$).

The most notable aspect of this variation is the highest Galactic NS-NS merger rate: 65.9 Myr^{-1} for submodel A

and sub-solar metallicity. When compared to the standard model, these systems merge ~ 8 times more often (from 8.1 Myr^{-1} to 65.9 Myr^{-1}). In this variation the λ is smaller (by at least factor of 2) than the one used in the standard model for a NS progenitor (typically a $10 M_{\odot}$ star; see Fig. 1). It means that the envelope is strongly bound in V2. As a consequence the binaries will end the CE with smaller orbital separations than they would in the standard model. This effect is additionally enhanced since NS-NS progenitors, for $Z = 0.1 Z_{\odot}$, often experience two CE events (see NSNS01 in Tab. 5 in standard model; a similar channel is also found in V2). A decreased semi-major axis increases the chances of survival through a SN. The vast majority of disruptions occur corresponding to the first SN, when the systems are still wide. For example, in the standard model $\sim 94\%$ of disruptions are encountered at the first SN, while $\sim 6\%$ at the second SN. In V2, there are virtually no disruptions at the second SN leading to the 8-fold increase of merger rates. A secondary effect of the strongly bound envelope is the migration of the progenitors toward low merger times. This has two competing consequences. One is the increased number of mergers during CE and a moderate reduction of merger rates. The second is the efficient dissipation of orbital energy that allows wide progenitors (that in the standard model would produce non-merging NS-NS) to form merging NS-NS systems moderately increasing the merger rates.

For solar metallicity the effect of SN survival does not manifest itself because progenitors of NSs often experience ECSe (high wind mass loss reduces pre-SN progenitor mass), which generally do not disrupt binaries (no kick). However, for Z_{\odot} there is a significant NS-NS merger rate drop in submodel B (from 7.6 Myr^{-1} in the standard model to 1.1 Myr^{-1} in this variation). The main formation channel in the standard model (see NSNS01 in Table 4) involves a CE and non-conservative mass transfer after the first SN. In V2 after the CE the orbital separation is smaller than in the standard model. Therefore the secondary, a low mass helium star that is a progenitor of the second NS, experiences RLOF much earlier in its evolution in V2. A combination of shorter orbital period and the earlier evolutionary stage (typically helium HG) leads to the development of the second CE in V2 (as opposed to stable mass transfer in the standard model). Since the survival through CE with HG donors is not allowed in model B, the merger rates significantly decrease. There is also a small decrease of merger rates in submodel A. Although HG CE is allowed in submodel A, small orbital separation in V2 sometimes leads to a merger in the second CE event.

The most notable change in the merger rates of BH-NS systems is the drop for $Z = 0.1 Z_{\odot}$: $3.4\text{--}0.5 \text{ Myr}^{-1}$ (standard–this variation) for submodel A and $2.3\text{--}0.4 \text{ Myr}^{-1}$ for submodel B. This comes from the fact that, for low metallicity environments, the progenitors of BH-NS systems quite often engage in a CE at the beginning of their evolution (see BHNS01 in Tab. 5). In this early CE event, the donor is the more massive component and a progenitor of the BH. The λ value used in this variation (0.1) is higher than in the standard model for a BH progenitor (see Fig. 3.4). This means that the envelope is easier to eject and after the first CE the binaries will

not lose as much orbital energy remaining above the 10 Gyr merger time. Additionally a wider separation after the first CE increases the chances of disruption by the supernovae. A combination of both effects accounts for the drop in BH-NS merger rates for both submodels for $Z = 0.1 Z_{\odot}$. This does not manifest itself for the $Z = Z_{\odot}$ model. High wind mass loss rates present at solar metallicity often reduce the initial mass ratio of the progenitors ($\gtrsim \frac{1}{2}\text{--}\frac{1}{3}$) and the first interaction instead of being a CE is a non-conservative mass transfer (see BHNS01 in Tab. 4). Since λ plays role on in CE events, the BH-NS rates are comparable in V2 and the standard model. The factor of ~ 2 difference arises from the later CE events initiated by the NS progenitor.

For solar metallicity the BH-BH merger rates increase by a factor of ~ 2 (from 8.2 Myr^{-1} to 15.3 Myr^{-1}) for submodel A, and decrease by factor of ~ 5 (from 1.9 Myr^{-1} to 0.4 Myr^{-1}) for submodel B, in contrast with the standard model. The λ value fixed in this variation (at 0.1) is larger than the average *Nanjing* values for typical BH progenitors (see Figs. 3 and 4). High λ and correspondingly low binding energy leads to small orbital contraction during the CE phase. This can (counter-intuitively) both increase and decrease merger rates of various BH-BH populations. For example, consider BH-BH populations in submodel A and B. From the relative merger rates (A much higher than B) it is clear that submodel A is dominated by BH-BH binaries that evolved through the CE phase with a HG donor. In contrast, submodel B includes only systems that have formed through CE with a CHeB donor (by assumption). Since HG stars are smaller (for the same mass and metallicity) than CHeB stars, progenitors in submodel A have relatively small orbital separations, while in submodel B they have relatively wide separations. On one hand, short period progenitor binaries do not merge in the CE phase as often as in the standard model, since the λ chosen in V2 is large, and that leads to an increased BH-BH merger rate in submodel A. On the other hand, long period progenitor binaries are not sufficiently contracted (in term of separation) due to the high λ in V2. They form long-period BH-BH systems with merger times exceeding 10 Gyr, and thus the merger rate decreases in submodel B. For sub-solar metallicity the effects of an increased λ are compensated for by the smaller radial expansion of stars as compared to solar metallicity, and the V2 merger rates for both submodels are similar to the standard model rates.

The distribution of chirp masses for both submodels and metallicities closely resembles that of the standard model. The average chirp masses for $Z = Z_{\odot}$ are $1.08\text{--}1.06 M_{\odot}$ (submodel A–B) for NS-NS, $3.2\text{--}3.2 M_{\odot}$ for BH-NS, and $6.5\text{--}6.5 M_{\odot}$ for BH-BH systems. For $Z = 0.1 Z_{\odot}$ the corresponding values are $1.09\text{--}1.07 M_{\odot}$ (submodel A–B) for NS-NS, $3.5\text{--}3.3 M_{\odot}$ for BH-NS, and $17.2\text{--}9.3 M_{\odot}$ for BH-BH systems.

The average values of delay times for Z_{\odot} are: $90\text{--}618 \text{ Myr}$ (submodel A–B) for NS-NS, $2.2\text{--}2.6 \text{ Gyr}$ for BH-NS, and $1.8\text{--}6.5 \text{ Gyr}$ for BH-BH systems. For $0.1 Z_{\odot}$ the values are: $0.2\text{--}1.6 \text{ Gyr}$ (NS-NS), $1.6\text{--}1.7 \text{ Gyr}$ (BH-NS), $1.2\text{--}1.9 \text{ Gyr}$ (BH-BH systems).

This variation fixes the binding to $\lambda = 1$. The Galactic merger rates for Z_{\odot} are dominated by NS-NS systems (48.8–14.3 Myr^{-1} , submodel A–B) followed by BH-BH (5.0–0.03 Myr^{-1}) and BH-NS systems (4.6–0.03 Myr^{-1}). For sub-solar metallicity, the BH-BH systems merge most often (90.2–7.9 Myr^{-1} , submodel A–B), then NS-NS systems (44.1–4.2 Myr^{-1}) and BH-NS systems (15.8–8.4 Myr^{-1}).

For solar metallicity there are no significant changes in merger rates for submodel A. However, the rise in rates for NS-NS systems by a factor of ~ 2 when compared to the standard model (from 23.5 Myr^{-1} to 48.8 Myr^{-1}) makes it the most frequently merging population of double NSs, for Z_{\odot} , in this study. The increase of merger rates for NS-NS and BH-NS systems (from 1.6 Myr^{-1} to 4.6 Myr^{-1}) is associated with fewer binaries merging during the CE due to the high λ value used in this variation. However, the high λ values have the opposite effect for BH-BH systems. The resulting low binding energy of the CE is responsible for the slight drop in merger rates for BH-BH systems (from 8.2 Myr^{-1} to 5.0 Myr^{-1}), as fewer binaries cross the 10 Gyr point (toward the merging population) due to insufficient orbital energy loss when ejecting their envelopes.

The population of NS-NS systems in submodel B follows the behaviour described in submodel A. What is noticeable for BH-NS and BH-BH systems in submodel B, at Z_{\odot} , is a drop in the merger rates (by an order of magnitude with respect to the standard model). By assumption, submodel B favours DCOs which initiated a CE with a donor beyond the HG, in this case during CHeB. Donors of this type that are progenitors of components in BH-NS or BH-BH systems have lower (see Figs. 2–4) λ values in the standard model (more physical) than in this variation ($\lambda = 1$). A direct consequence is the reduced orbital energy loss during a CE event. This allows binaries with CHeB CE to retain a large separation at the end of the CE phase, preventing a DCO merger within 10 Gyr. Therefore, the population of merging DCOs containing BHs for submodel B is reduced.

For sub-solar metallicities the high λ effect is still relevant. However, in these chemical environments donors initiate CE more often as CHeB stars (instead of HG) due to smaller radial expansion during the evolution. This increases the number and merger rates of NS-NS and BH-NS systems in submodel B. This also allows for more BH-BH systems to be formed in this submodel but for this type of DCO the high λ causes a counter-effect, and efficiently reduces the merger rates of double BHs.

The average chirp masses for Z_{\odot} are: 1.06–1.05 M_{\odot} (submodel A–B) for NS-NS, 2.7–2.4 M_{\odot} for BH-NS, and 6.0–5.9 M_{\odot} for BH-BH systems. For 0.1 Z_{\odot} the values are: 1.09–1.12 M_{\odot} for NS-NS, 2.9–2.9 M_{\odot} for BH-NS, and 12.5–6.8 for BH-BH systems.

The average delay times for Z_{\odot} are: 1.2–2.2 Gyr (submodel A–B) for NS-NS, 2.0–2.7 Gyr for BH-NS, and 4.2–2.2 Gyr for BH-BH systems. The values for 0.1 Z_{\odot} are: 0.9–2.4 Gyr for NS-NS, 1.8–2.3 Gyr for BH-NS, and 1.6–3.3 Gyr for BH-BH systems. These average values are greater than for the standard model, as the high λ value used in this variation (low binding energy) allows the binaries to retain a larger orbital separation after the CE phase.

4.5. Variation 4

In this model we fix the λ value at 10. The Galactic merger rates for Z_{\odot} are: 20.8–0.3 Myr^{-1} (submodel A–B) for NS-NS, 0.9–0.0 Myr^{-1} for BH-NS, and 0.3–0.0 Myr^{-1} for BH-BH systems. The rates for 0.1 Z_{\odot} are: 29.5–1.4 Myr^{-1} for NS-NS, 8.8–1.6 Myr^{-1} for BH-NS, and 5.9–0.3 Myr^{-1} for BH-BH systems.

For Z_{\odot} the populations of DCOs of all types experience a reduction in the merger rate for both submodels (see Table 2) when compared with the standard model. The mechanism responsible for this result is straightforward. The very high λ value means a low binding energy of a star’s envelope, and so it is easily ejected during a CE event. As a consequence, little orbital energy is lost, and the separation of the components is reduced insignificantly. The weak orbital contraction causes the DCOs to retain merger times larger than 10 Gyr, thus creating a large non-merging population at the cost of the merging one. The mechanism described above holds true for all types of DCOs, but manifests most clearly for BH-BH systems. For example, for submodel A, for each BH-BH system formed below the 10 Gyr merger time limit, ~ 240 are formed above it. For submodel B the rates are null for BH-NS and BH-BH systems. In other words, despite high statistics—6 million binary stars simulated—no DCO systems containing BHs were produced. In order to understand this result one needs to recall that the CE phase is usually initiated by HG and CHeB donors, due to significant radial expansion during these stages of evolution. Submodel B does not allow for a HG donor so the only systems left to populate this submodel are those with a CHeB donor during the CE, in their evolutionary history. This evolved CE donor indicates that these binaries had initial separations large enough to be able to bypass the CE on the HG, and this initial orbital condition places them in the long merger time regime. For progenitors of BH-NS and BH-BH systems the λ value in the standard model during CHeB is much lower (see Figs. 2–4) when compared to the one used in this variation (10). So, due to insufficient orbital energy loss during CE, no binaries are drawn toward the merging population, making it void of system containing BHs. This migration of DCOs between the merging and non-merging populations is illustrated in Figure 18.

For 0.1 Z_{\odot} more merging BH-NS/BH systems are formed in general due to weaker SNe (see Sec. 4.1). The probability of producing such a system for the merging population increases, yielding non-zero merger rates for submodel B. Additionally, the merger rates for BH-NS system for submodel A increase by a factor of ~ 3 (from 3.4 to 8.8 Myr^{-1}) when contrasted with the standard model. This result is opposite to the one for Z_{\odot} , where the merger rate of BH-NS systems for submodel A drops slightly (from 1.6 to 0.9 Myr^{-1}). A weakly bound CE (in this variation) causes insignificant orbital reduction and increases the chances of disruption by the following SNe (after the first or second CE, see Table 5). However the stalled SN kicks associated with low metallicity environments reduce the disruption probability, accounting for the increase in 0.1 Z_{\odot} in V4.

For NS-NS systems the Galactic merger rates increase from 8.1 Myr^{-1} (standard model) to 29.5 Myr^{-1} (this variation) at 0.1 Z_{\odot} . A characteristic of these DCOs for

sub-solar metallicities is the second CE initiated just after the first one (see Table 5). Two weakly bound CE phases allow the binary to avoid a merger in either of these events, effectively increasing the number and merger rates of NS-NS systems.

The average chirp masses for Z_{\odot} are $\sim 1.03 M_{\odot}$ for both submodels for NS-NS systems. For BH-NS and BH-BH systems, submodel A, these are: $2.5 M_{\odot}$ and $5.8 M_{\odot}$, respectively. For $0.1 Z_{\odot}$ these values are: $1.1\text{--}1.2 M_{\odot}$ (submodel A–B) for NS-NS, $2.9\text{--}2.7 M_{\odot}$ for BH-NS, and $7.6\text{--}6.7 M_{\odot}$ for BH-BH systems.

The average delay time values for Z_{\odot} , for NS-NS systems are 0.5 Gyr and 2.0 Gyr, for submodel A and B, respectively. For BH-NS and BH-BH systems these are 2.5 Gyr and 3.2 Gyr, respectively, for submodel A. For $0.1 Z_{\odot}$ these values are: $0.7\text{--}2.0$ Gyr (submodel A–B) for NS-NS, $2.4\text{--}2.2$ Gyr for BH-NS, and $3.8\text{--}2.7$ for BH-BH systems.

4.6. Variation 5 & 6

In variations 5 and 6 we set the maximum mass achievable for a NS to $3.0 M_{\odot}$ and $2.0 M_{\odot}$, respectively (this is $2.5 M_{\odot}$ in the standard model). These models produce no statistically significant changes, when compared to the standard model. The reason for the population of DCOs being insensitive to the maximum mass of a NS is the usage of the Rapid supernova mechanism. The main characteristic of this engine is the lack of compact objects formed in the range $\sim 2\text{--}5 M_{\odot}$.

The distribution of delay times and chirp masses, as well as their average values, are nearly identical (within statistical accuracy) to the standard model.

4.7. Variation 7

In this variation we set the σ of the Maxwellian distribution of the natal kicks to 132.5 km/s (it is 265 km/s in the standard model). The Galactic merger rates for Z_{\odot} are: $32.4\text{--}9.5$ Myr $^{-1}$ (submodel A–B) for NS-NS, $1.9\text{--}0.3$ Myr $^{-1}$ for BH-NS, and $10.4\text{--}2.1$ Myr $^{-1}$ for BH-BH systems. For sub-solar metallicity the rates are: $8.3\text{--}2.2$ Myr $^{-1}$ for NS-NS, $6.1\text{--}4.3$ Myr $^{-1}$ for BH-NS, and $83.7\text{--}15.1$ Myr $^{-1}$.

For solar metallicity we find slightly increased (by less than a factor of ~ 2) Galactic rates for all DCO types, for both submodels. In practice, reducing the σ value means that natal kicks of high magnitude are chosen less frequently from the Maxwellian distribution. As a consequence fewer binaries are disrupted during the SN explosions. This increases the pool of potential merging DCOs, and accounts for higher merger rates in this variation. The least affected, when compared to the standard model, are BH-BH systems, since the progenitors of these systems are massive stars, and thus produce weak SNe (stalled or no kicks, direct collapse). Therefore, statistically, these systems are minimally impacted by decreasing the occurrence of high magnitude natal kicks in the binary population.

For sub-solar metallicity this effect is even less significant, due to naturally weaker explosions. Low wind mass loss rates associated with low metallicity environments produce more massive pre-SN progenitors. These stars cause more fallback of ejecta during the explosion, due to their strong gravitational potential. Therefore, the magnitude of the velocity of the kicks is in general smaller

than for Z_{\odot} . Further reduction of the occurrence of high magnitude kicks yields no statistically significant effects.

In the case of NS-NS systems for $0.1 Z_{\odot}$ the rates are almost unchanged when compared with the standard model. Note that most of these DCOs have two CE events (exactly like in the standard model, see Table 5), which makes them susceptible to merging during one of these episodes. Reducing the probability of high velocity kicks results in smaller separations after the first SN. A consequence is an increased number of CE mergers that counters increased SN survivability.

The average chirp masses for Z_{\odot} are: $1.05 M_{\odot}$ for NS-NS, $3.1 M_{\odot}$ for BH-NS, and 6.6 for BH-BH systems (all for both submodels). For $0.1 Z_{\odot}$ the values are: $1.08 M_{\odot}$ for NS-NS and $3.1 M_{\odot}$ for BH-NS systems (for both submodels). For BH-BH systems these are: $12.4 M_{\odot}$ for submodel A and $9.7 M_{\odot}$ for submodel B.

The average values of delay time distribution are: $1.3\text{--}2.2$ Gyr (submodel A–B) for NS-NS, $2.7\text{--}4.3$ Gyr for BH-NS, and $1.2\text{--}2.9$ Gyr for BH-BH systems. For $0.1 Z_{\odot}$ the values are: $1.0\text{--}2.7$ Gyr for NS-NS, $1.9\text{--}1.9$ Gyr for BH-NS and $1.1\text{--}1.3$ Gyr for BH-BH systems.

4.8. Variation 8

In this model we only enforce full natal kicks for the BHs. The results therefore only change for BH-BH/NS systems. The Galactic merger rates for Z_{\odot} for BH-NS systems are $0.03\text{--}0.004$ Myr $^{-1}$ (submodel A–B). For BH-BH systems: $0.05\text{--}0.005$ Myr $^{-1}$. For $0.1 Z_{\odot}$ the rates are: $0.7\text{--}0.2$ Myr $^{-1}$ for BH-NS and $4.2\text{--}0.8$ Myr $^{-1}$ for BH-BH systems.

The disruption rate of binary progenitors of BH-BH/NS systems during the SN, due to the strong velocity kicks, is significant. When contrasted with the standard model, the Galactic merger rates for Z_{\odot} drop by 2–3 orders of magnitude (see Table 2). For example, for BH-BH, submodel B at Z_{\odot} , the merger rate drops from 1.9 Myr $^{-1}$ (standard) to 0.005 Myr $^{-1}$. For $0.1 Z_{\odot}$ the effect is smaller but still noticeable, as the rates drop by a factor of ~ 10 (see Table 3). The pre-SN progenitors of BHs in this environment are, on average, more massive when compared to Z_{\odot} . This results in strongly bound binaries, which makes them less susceptible to being disrupted from natal kicks.

The average chirp masses for Z_{\odot} are: $3.0\text{--}3.2 M_{\odot}$ (submodel A–B) for BH-NS systems. For BH-BH systems these are $6.5 M_{\odot}$ and $5.9 M_{\odot}$ for submodels A and B, respectively. For $0.1 Z_{\odot}$ these values are $1.09 M_{\odot}$ (both submodels) for NS-NS systems and $3.0 M_{\odot}$ (also both submodels) for BH-NS systems. For BH-BH systems these are $9.0 M_{\odot}$ and $7.2 M_{\odot}$ for submodels A and B, respectively.

The mean delay times for Z_{\odot} are: $1.2\text{--}1.7$ Gyr (submodel A–B) for NS-NS systems and $2.0\text{--}7.0$ Gyr for BH-BH systems. For BH-NS, submodel A, the mean value is 0.4 Gyr. For $0.1 Z_{\odot}$ the mean values are: $0.9\text{--}2.2$ Gyr (submodel A–B) for NS-NS, $1.2\text{--}1.3$ Gyr for BH-NS, and $0.6\text{--}1.2$ Gyr for BH-BH systems.

4.9. Variation 9

In this variation BHs do not receive natal kicks. We therefore describe the results for BH-NS and BH-BH systems (NS-NS systems behave as in the standard model). The Galactic merger rates for BH-NS systems are 1.4--

0.2 Myr⁻¹ (submodel A–B) for Z_{\odot} and 5.2–3.7 Myr⁻¹ (0.1 Z_{\odot}). For BH-BH systems the rates are: 16.9–4.2 Myr⁻¹ (Z_{\odot}) and 92.3–19.3 Myr⁻¹ (0.1 Z_{\odot}).

For Z_{\odot} the merger rates for BH-BH systems increase by a factor of ~ 2 for both submodels, when compared to the standard model. This is a straightforward consequence of the assumption of no natal kicks used in this variation. The survival rate of BH-BH/NS systems increases due to fewer disruptions occurring during the SN. This allows more DCOs with BHs, which in turn increases the merger rates. For 0.1 Z_{\odot} the gain is smaller. Pre-SN progenitors of BHs are heavier in this chemical environment due to low wind mass loss. This causes a lot of ejecta fallback (almost all matter is pulled back onto the newly formed BH). Setting no natal kicks for these systems changes little as these BHs “naturally” suppress the SN explosion.

The behaviour of BH-NS systems is explained analogously to BH-BH DCOs. However the effects are smaller since the survival rates due to disruption are dominated by SNe resulting in the formation of NSs. Pre-SN progenitors of NSs are light and experience low fallback (stronger kicks). This allows for more powerful explosions, which disrupt the binaries and prevent the creation of DCOs.

The average chirp masses for BH-NS systems are: 3.1 M_{\odot} for Z_{\odot} and 3.0 M_{\odot} for 0.1 Z_{\odot} (all for both submodels). For BH-BH systems the values are: 6.3–6.2 M_{\odot} (submodel A–B) for Z_{\odot} and 12.1–9.3 M_{\odot} for 0.1 Z_{\odot} .

The mean values of delay times for BH-NS systems are: 1.7–3.0 Gyr (submodel A–B) for Z_{\odot} and 1.7–1.7 Gyr (0.1 Z_{\odot}). For BH-BH systems these are: 1.5–3.4 Gyr for Z_{\odot} and 1.2–1.4 Gyr for 0.1 Z_{\odot} .

4.10. Variation 10

In this variation we use the Delayed supernova engine (as compared with the Rapid engine used in the standard model). The Galactic merger rates for Z_{\odot} are: 25.6–8.9 Myr⁻¹ (submodel A–B) for NS-NS, 0.07–0.03 Myr⁻¹ for BH-NS, and 0.6–0.08 Myr⁻¹ for BH-BH systems. For 0.1 Z_{\odot} the rates are: 8.6–2.6 Myr⁻¹ for NS-NS, 2.3–2.0 Myr⁻¹ for BH-NS, and 62.0–11.5 Myr⁻¹ for BH-BH systems.

For all metallicities and submodels we note a drop in the merger rates for systems containing BHs (see Table 2 and 3). The reason for this is the difference in the amount of fallback matter acquired in SN explosions resulting from the two engines. To illustrate, we present the results of an example calculation using Eq. 16, 18, and 19 from Fryer et al. (2011), estimating the fallback factor f_{fb} . For a star prior to the SN explosion with a total mass $M = 8.7 M_{\odot}$ and carbon-oxygen core $M_{\text{CO}} = 6.5 M_{\odot}$ (typical core mass collapsing to a BH), we get the following values of f_{fb} : 1.0 (full fallback) for the Rapid and 0.46 (partial fallback) for the Delayed engine. For progenitors of BHs the amount of fallback is lower (more mass is ejected) in the case of the Delayed engine. This results in natal kicks of a higher magnitude (see Eq. 3), which are more capable of disrupting the binary and preventing the creation of a DCO. For progenitors of NSs the fallback is similar in both V10 and the standard model, and therefore we find similar magnitudes of natal kicks, and a similar chance for disruption by SN.

Another significant result produced by this model is the

lower limit of the chirp mass distribution for BH-BH systems: ~ 2 (for an example see Figure 10). The Delayed supernova engine creates remnant objects (NSs and BHs) with a continuous spectrum of masses, contrary to the Rapid engine (for details see Belczynski et al. (2011b)). This suggests observational tests to distinguish the models (Fryer et al., 2011; Belczynski et al., 2011b).

The average chirp mass for Z_{\odot} is: 1.14–1.13 M_{\odot} (submodel A–B) for NS-NS, 3.1–3.0 M_{\odot} for BH-NS, and 5.7–4.6 M_{\odot} for BH-BH systems. For 0.1 Z_{\odot} these are: 1.2–1.2 M_{\odot} for NS-NS, 3.4–3.4 M_{\odot} for BH-NS, and 14.4–10.2 M_{\odot} for BH-BH systems.

The mean delay time values for Z_{\odot} are: 1.2–1.8 Gyr (submodel A–B) for NS-NS, 2.5–1.4 Gyr for BH-NS, and 1.7–2.6 Gyr for BH-BH systems. For 0.1 Z_{\odot} these are: 0.9–2.1 Gyr for NS-NS, 1.8–1.7 Gyr for BH-NS, and 1.2–1.5 Gyr for BH-BH systems.

4.11. Variation 11

In this variation we reduce the stellar wind mass loss rates by a factor of 2. The Galactic merger rates for Z_{\odot} are: 24.2–6.5 Myr⁻¹ (submodel A–B) for NS-NS, 1.2–0.2 Myr⁻¹ for BH-NS, and 29.7–3.6 Myr⁻¹ for BH-BH systems. For 0.1 Z_{\odot} the rates are: 7.7–2.3 Myr⁻¹ for NS-NS, 3.8–2.4 Myr⁻¹ for BH-NS, and 79.2–17.1 for BH-BH systems.

The most significant result due to this variation is the increase in the Galactic merger rate for BH-BH systems for Z_{\odot} . The rates increase by a factor of ~ 3 and ~ 2 for submodels A and B, respectively. The effect of the lowered wind mass loss rates on double BHs is manifold. First, the decreased reduction of mass of BH progenitors causes them to retain more mass just prior to the SN. This results in a larger amount of fallback matter during the explosion, which stalls the natal kicks. This in turn increases the survivability rate of binaries and produces more merging systems. Second, the increased pre-SN mass also results in more massive remnants, which is clearly visible in Figure 10 and 11. Third, the minimum mass of a BH progenitor is reduced to lower values (from the usual $\sim 20 M_{\odot}$ to $\sim 18 M_{\odot}$). For sub-solar environments these effects are weak as the wind mass loss rate for 0.1 Z_{\odot} is already low. Decreasing this even further yields no new qualitative results.

For NS-NS systems these effects are also insignificant. The progenitors of NSs in these systems are lighter than those of BHs, and for these stars the wind mass loss rates are smaller than for their heavier counterparts. Therefore, decreasing wind mass loss even further plays no significant role in the survivability or the properties of these systems.

The merger rates for BH-NS systems do not increase in the way they do for BH-BH systems, despite their harboring a BH and a massive NS progenitor. Binary stars that would have formed BH-NS systems in the case of “standard” winds, now retain more mass during evolution (due to the reduced winds), and form BH-BH systems instead. This reduces the BH-NS population and adds merging DCOs to the BH-BH systems.

The average chirp masses for Z_{\odot} are: 1.05–1.05 M_{\odot} (submodel A–B) for NS-NS, 3.2–3.3 M_{\odot} for BH-NS, and 10.5–9.1 M_{\odot} for BH-BH systems. Note that for the latter DCOs the range of chirp mass is the largest ($\sim 14 M_{\odot}$) for this metallicity of all variations. For 0.1 Z_{\odot} the average

chirp masses are: 1.08–1.08 M_{\odot} for NS-NS, 3.3–3.4 M_{\odot} for BH-NS, and 14.3–10.6 M_{\odot} for BH-BH systems.

The mean delay times for Z_{\odot} are: 1.0–1.6 Gyr (submodel A–B) for NS-NS, 1.3–1.9 Gyr for BH-NS, and 0.6–2.8 Gyr for BH-BH systems. For 0.1 Z_{\odot} these values are: 1.0–2.3 Gyr for NS-NS, 1.5–1.5 Gyr for BH-NS, and 1.0–1.2 Gyr for BH-BH systems.

5. SUMMARY

We have investigated the major parameters and input physics involved in binary evolution leading to the formation of double compact objects: the CE coefficient λ , the supernova mechanisms (remnant formation and natal kick magnitude), the maximum mass of NSs, and the wind mass loss rates. The study was performed by calculating a suite of population synthesis models, allowing us to estimate the associated uncertainties in the formation of DCOs.

The calculations were done using the **StarTrack** population synthesis code, recently updated with wind mass loss rates for massive stars, a realistic CE treatment, and convection-driven neutrino-enhanced supernovae. These updates are incorporated in our revised Standard Model (see Section 4.1) of binary evolution and DCO formation. Our newer version yields lower merger rates than the equivalent Standard Model from Belczynski et al. (2002). This difference arises mainly from the *Nanjing* treatment of the CE parameter, λ (see Section 2.3.2; Xu & Li (2010)), which we have now incorporated. Significant changes in the merger rates are also caused by varying the value of λ (Variations 1–4, see Table 2 and 3). We therefore identify a strong dependence of the merger rates on the binding energy of the CE.

Emerging from the simulations are two populations of DCOs. The first is that of double compact objects with merger times less than 10 Gyr (merging in a Milky Way-like galaxy, the *merging population*). The second is of objects having merger times higher than this limit (distant future mergers, the *non-merging population*). The λ parameter shifts DCOs between these two populations. On the one hand, lowering λ increases the CE binding energy, and thus tends to draw the binaries from the non-merging population toward the merging one, as progenitor binaries must lose more orbital energy to unbind the envelope. This results in a larger number of system in the merging population, and increases the Galactic merger rates. On the other hand, this also causes progenitors of DCOs from the merging population to merge during the CE more often, terminating binary evolution and therefore reducing the number of binary systems, and thus merger rates. The final outcome is set by the specific value of λ , and varies from population to population. For example, a given change in λ may cause an increase in the merger rate of BH-BH systems while decreasing the rate of NS-NS systems, due to the differing orbital separations of BH-BH and NS-NS progenitors.

The types of DCOs most affected by this mechanism are NS-NS and BH-NS systems. The range of merger rates for these systems spans three orders of magnitude between solar and sub-solar metallicities (see Table 2 and Table 3). The large range of merger rates obtained in this and previous studies using calculations with a fixed value of λ is

an artifact of the unphysical treatment of the CE phase. When a more physically motivated treatment is applied, in which the value of λ is chosen to correspond to the given star and its evolutionary stage, it is found that the merger rates are on the high side of the ranges computed with variations that assume non-physical, fixed values of λ .

In particular, for the standard model, for either choice of metallicity of submodel (A or B), the BH-BH Galactic merger rate is at least 1.9 per Myr. This is a factor of ~ 5 higher than the “realistic” estimate used in Abadie et al. (2010), which translates into a detection rate of 20 BH-BH mergers per year with Advanced LIGO and Virgo detectors in that paper. Therefore, if the standard model is correct, we may expect that advanced gravitational-wave detectors will be able to capture above a hundred BH-BH coalescences per year. This is a clearly positive prediction from the perspective of the ongoing searches for gravitational-wave signals. However, we are unable to provide an error estimate on this improvement, since there are no alternative physical estimates for λ readily available to us. Therefore, one should treat this estimate with some caution.

We can test the validity of certain models using the observed limits on the Galactic NS-NS merger rate (Kim et al., 2006). Their upper limit (190 Myr^{-1}) is not violated by any of our models. However, the lower limit (3 Myr^{-1}) is not met by several of our models, and they would therefore be ruled out. Models (for Z_{\odot}) that do not meet this condition are: Variation 1-submodel A (NS-NS Galactic merger rate 0.4 Myr^{-1}), Variation 1-submodel B (0.4 Myr^{-1}), Variation 2-submodel B (1.1 Myr^{-1}), and Variation 4-submodel B (0.3 Myr^{-1}); this is illustrated in Figure 19. All these variations employ a fixed value of λ , and the observations of Galactic NS-NS systems lend further support to our claim that such a treatment is unphysical. Additionally we can use the estimates on the predicted chirp mass of IC10 X–1 (0.3 Z_{\odot} environment) to further validate our results. We test our chirp mass distribution for 0.1 Z_{\odot} against the predicted minimal predicted chirp mass for IC10 X–1 equal to 15 M_{\odot} (Bulik et al., 2011). From Fig. 13 and Table 9 one can see that models V3-submodel B (max. chirp mass 14.9 M_{\odot}) and V4-submodel B (max. chirp mass 11.5 M_{\odot}) do not reach this limit. Again these models use constant, in this case high λ values. This is further evidence to support the claim that such a treatment is unphysical.

Another influential factor in DCO formation is the treatment of SN explosions. Specifically, the magnitude of the natal kick plays a significant role, as the high kicks (assumed in our standard model) tend to disrupt DCO progenitors, reducing the merger rates. The rates for reduced (by half) kicks are given in model V7. The corresponding increase in the rates is rather modest, due to the fact that for NS-NS systems some NSs explode as electron capture supernovae and do not receive kicks at all. BH kicks are already reduced by the amount of fall back and further kick decrease (coming from reducing σ in V7) does not significantly increase the rates. However, the effect of kicks becomes significant for BH-BH systems once the assumption on the reduction of kicks by fallback is relaxed. We have allowed for the very wide range of possible BH kicks in models V8 (high kicks) and V9 (no kicks). It is found

that the Galactic merger rates of BH-BH systems change by $\sim 2-3$ orders of magnitude (see Table 2, 3). Therefore, the mostly unknown magnitude of BH natal kick limits our predictive power for the BH-BH rate estimates.

Despite the fact that we lack strong observational or theoretical constraints on BH natal kicks, in our standard model we have adopted the most likely model of natal kicks (ones that decrease with increasing BH mass). This model is supported by existing observations (most massive BHs seem to form without a kick) and can be intuitively understood in the framework of natal kicks arising from asymmetric supernova mass ejection. The standard model BH-BH merger rates are close to upper limit set by the full allowed range of possibilities (V8–V9), and again it appears that our more realistic treatment of DCO formation favors higher rates, and sets an optimistic tone for near-future gravitational wave inspiral detection.

This is the first in a series of three papers. Results presented here, and their extensions in the *Synthetic Universe* on-line database (www.syntheticuniverse.org), will be used in the sec-

ond study, where we will investigate the NS-NS/BH-NS/BH-BH merger rates as a function of cosmological redshift, star formation rate, and metallicity. The third paper will focus on gravitational wave detection rates for upcoming observatories (advanced LIGO/Virgo and Einstein Telescope).

We would like to thank the N. Copernicus Astronomical Centre in Warsaw, Poland, for their courtesy in enabling us to use their computational resources. Work at LANL was done under the auspices of the National Nuclear Security Administration of the U.S. Department of Energy at Los Alamos National Laboratory under Contract No. DE-AC52-06NA25396. EB is supported by NSF Grant PHY-0900735 and by NSF CAREER Grant PHY-1055103. ROS is currently supported by NSF award PHY-0970074, the Bradley Program Fellowship, and the UWM Research Growth Initiative. TB is supported by the Polish grants N N203 511238 and DPN/N176/VIRGO/2009 KB is supported by the Polish grant N N203 302835. MD is supported by the Polish grant GR-4071.

REFERENCES

- Abadie, J., Abbott, B. P., Abbott, R., Abernathy, M., Accadia, T., Acernese, F., Adams, C., Adhikari, R., Ajith, P., Allen, B., & et al. 2010, *Classical and Quantum Gravity*, 27, 173001
- Abt, H. A. 1983, *ARA&A*, 21, 343
- Bailyn, C. D., Jain, R. K., Coppi, P., & Orosz, J. A. 1998, *ApJ*, 499, 367
- Belczynski, K., Bulik, T., Fryer, C. L., Ruiter, A., Valsecchi, F., Vink, J. S., & Hurley, J. R. 2010a, *ApJ*, 714, 1217
- Belczynski, K., Bulik, T., & Rudak, B. 2004, *ApJ*, 608, L45
- Belczynski, K., Dominik, M., Bulik, T., O’Shaughnessy, R., Fryer, C., & Holz, D. E. 2010b, *ApJ*, 715, L138
- Belczynski, K., Kalogera, V., & Bulik, T. 2002, *ApJ*, 572, 407
- Belczynski, K., Kalogera, V., Rasio, F. A., Taam, R. E., Zezas, A., Bulik, T., Maccarone, T. J., & Ivanova, N. 2008, *ApJS*, 174, 223
- Belczynski, K., Lorimer, D. R., Ridley, J. P., & Curran, S. J. 2010c, *MNRAS*, 407, 1245
- Belczynski, K., Perna, R., Bulik, T., Kalogera, V., Ivanova, N., & Lamb, D. Q. 2006, *ApJ*, 648, 1110
- Belczynski, K., & Taam, R. E. 2008, *ApJ*, 685, 400
- Belczynski, K., Taam, R. E., Kalogera, V., Rasio, F. A., & Bulik, T. 2007, *ApJ*, 662, 504
- Belczynski, K., Wiktorowicz, G., Fryer, C., Holz, D., & Kalogera, V. 2011a, *ArXiv e-prints*
- . 2011b, *ArXiv e-prints*
- Bodaghee, A., Tomsick, J. A., Rodriguez, J., & Berian James, J. 2011, *ArXiv e-prints*
- Bulik, T., Belczynski, K., & Prestwich, A. 2011, *ApJ*, 730, 140
- Chlebowski, T., & Garmany, C. D. 1991, *ApJ*, 368, 241
- Demorest, P. B., Pennucci, T., Ransom, S. M., Roberts, M. S. E., & Hessels, J. W. T. 2010, *Nature*, 467, 1081
- Dessart, L., Burrows, A., Ott, C. D., Livne, E., Yoon, S.-C., & Langer, N. 2006, *ApJ*, 644, 1063
- Dewi, J. D. M., & Pols, O. R. 2003, *MNRAS*, 344, 629
- Downing, J. M. B., Benacquista, M. J., Giersz, M., & Spurzem, R. 2010, *MNRAS*, 407, 1946
- Duquenois, A., & Mayor, M. 1991, *A&A*, 248, 485
- Farr, W. M., Sravan, N., Cantrell, A., Kreidberg, L., Bailyn, C. D., Mandel, I., & Kalogera, V. 2011, *ApJ*, 741, 103
- Fryer, C. L., Belczynski, K., Wiktorowicz, G., Dominik, M., Kalogera, V., & Holz, D. 2011, *ArXiv e-prints*
- Fryer, C. L., & Kalogera, V. 2001, *ApJ*, 554, 548
- Grindlay, J., Portegies Zwart, S., & McMillan, S. 2006, *Nature Physics*, 2, 116
- Gültekin, K., Miller, M. C., & Hamilton, D. P. 2004, *ApJ*, 616, 221
- Hamann, W.-R., & Koesterke, L. 1998, *A&A*, 335, 1003
- Heggie, D. C. 1975, *MNRAS*, 173, 729
- Herrero, A., Puls, J., & Najarro, F. 2002, *A&A*, 396, 949
- Hobbs, G., Lorimer, D. R., Lyne, A. G., & Kramer, M. 2005, *MNRAS*, 360, 974
- Humphreys, R. M., & Davidson, K. 1994, *PASP*, 106, 1025
- Hurley, J. R., Pols, O. R., & Tout, C. A. 2000, *MNRAS*, 315, 543
- Ivanova, N., Heinke, C. O., Rasio, F. A., Belczynski, K., & Fregeau, J. M. 2008, *MNRAS*, 386, 553
- Ivanova, N., & Taam, R. E. 2004, *ApJ*, 601, 1058
- Kim, C., Kalogera, V., & Lorimer, D. R. 2006, *ArXiv Astrophysics e-prints*
- Kobulnicky, H. A., & Fryer, C. L. 2007, *ApJ*, 670, 747
- Kroupa, P., Tout, C. A., & Gilmore, G. 1993, *MNRAS*, 262, 545
- Kroupa, P., & Weidner, C. 2003, *ApJ*, 598, 1076
- Kudritzki, R. P., Puls, J., Gabler, R., & Schmitt, J. H. M. M. 1991, in *Extreme Ultraviolet Astronomy*, ed. R. F. Malina & S. Bowyer, 130
- Lattimer, J. M., & Prakash, M. 2010, *ArXiv e-prints*
- Lépine, S., & Moffat, A. F. J. 2008, *AJ*, 136, 548
- Levine, A. M., Rappaport, S. A., & Zojcheski, G. 2000, *ApJ*, 541, 194
- Lorimer, D. R., McLaughlin, M. A., Arzoumanian, Z., Xilouris, K. M., Cordes, J. M., Lommen, A. N., Fruchter, A. S., Chandler, A. M., & Backer, D. C. 2004, *MNRAS*, 347, L21
- Loveridge, A. J., van der Sluys, M. V., & Kalogera, V. 2011, *ApJ*, 743, 49
- Markova, N., Puls, J., Repolust, T., & Markov, H. 2004, *A&A*, 413, 693
- Miller, M. C., & Lauburg, V. M. 2009, *ApJ*, 692, 917
- Mirabel, I. F., & Rodrigues, I. 2003, *Science*, 300, 1119
- Miyaji, S., Nomoto, K., Yokoi, K., & Sugimoto, D. 1980, *PASJ*, 32, 303
- Nelemans, G., Yungelson, L. R., & Portegies Zwart, S. F. 2001, *A&A*, 375, 890
- Nutzman, P., Kalogera, V., Finn, L. S., Hendrickson, C., & Belczynski, K. 2004, *ApJ*, 612, 364
- O’Leary, R. M., Rasio, F. A., Fregeau, J. M., Ivanova, N., & O’Shaughnessy, R. 2006, *ApJ*, 637, 937
- Orosz, J. A., McClintock, J. E., Aufdenberg, J. P., Remillard, R. A., Reid, M. J., Narayan, R., & Gou, L. 2011, *ArXiv e-prints*
- O’Shaughnessy, R., Kalogera, V., & Belczynski, K. 2005a, *ApJ*, 620, 385
- O’Shaughnessy, R., Kaplan, J., Kalogera, V., & Belczynski, K. 2005b, *ApJ*, 632, 1035
- O’Shaughnessy, R., Kim, C., Fragos, T., Kalogera, V., & Belczynski, K. 2005c, *ApJ*, 633, 1076
- Osterbrock, D., & Flather, E. 1959, *ApJ*, 129, 26
- Özel, F., Psaltis, D., Narayan, R., & McClintock, J. E. 2010, *ApJ*, 725, 1918
- Pfahl, E., Podsiadlowski, P., & Rappaport, S. 2005, *ApJ*, 628, 343
- Podsiadlowski, P., Langer, N., Poelarends, A. J. T., Rappaport, S., Heger, A., & Pfahl, E. 2004, *ApJ*, 612, 1044
- Prestwich, A. H., Kilgard, R., Crowther, P. A., Carpano, S., Pollock, A. M. T., Zezas, A., Saar, S. H., Roberts, T. P., & Ward, M. J. 2007, *ApJ*, 669, L21
- Repolust, T., Puls, J., & Herrero, A. 2004, *A&A*, 415, 349
- Sadowski, A., Belczynski, K., Bulik, T., Ivanova, N., Rasio, F. A., & O’Shaughnessy, R. 2008, *ApJ*, 676, 1162
- Silverman, J. M., & Filippenko, A. V. 2008, *ApJ*, 678, L17
- Vink, J. S., & de Koter, A. 2005, *A&A*, 442, 587

- Vink, J. S., de Koter, A., & Lamers, H. J. G. L. M. 2001, *A&A*, 369, 574
- Voss, R., & Tauris, T. M. 2003, *MNRAS*, 342, 1169
- Webbink, R. F. 1984, *ApJ*, 277, 355
- Wellstein, S., & Langer, N. 1999, *A&A*, 350, 148
- Wellstein, S., Langer, N., & Braun, H. 2001, *A&A*, 369, 939
- Wong, T.-W., Willems, B., & Kalogera, V. 2010, *ApJ*, 721, 1689
- Xu, X.-J., & Li, X.-D. 2010, *ApJ*, 716, 114

TABLE 1
SUMMARY OF MODELS^a

Model	Parameter	Description
S	Standard	$\lambda = \text{Nanjing}$, $M_{\text{NS,max}} = 2.5 M_{\odot}$, $\sigma = 265 \text{ km s}^{-1}$ BH kicks: variable, SN: Rapid
V1	$\lambda = 0.01$	very low λ : fixed
V2	$\lambda = 0.1$	low λ : fixed
V3	$\lambda = 1$	high λ : fixed
V4	$\lambda = 10$	very high λ : fixed
V5	$M_{\text{NS,max}} = 3.0 M_{\odot}$	high maximum NS mass
V6	$M_{\text{NS,max}} = 2.0 M_{\odot}$	low maximum NS mass
V7	$\sigma = 132.5 \text{ km s}^{-1}$	low kicks: NS/BH
V8	full BH kicks	high natal kicks: BH
V9	no BH kicks	no natal kicks: BH
V10	Delayed SN	NS/BH formation: Delayed SN engine
V11	weak winds	Wind mass loss rates reduced to 50%

^a All parameters, except for the one listed under “Description”, retain their Standard model (“S”) values.

TABLE 2
GALACTIC MERGER RATES, Z_{\odot} [Myr⁻¹]^a

Model	NS-NS	BH-NS	BH-BH
S	23.5 (7.6)	1.6 (0.2)	8.2 (1.9)
V1	0.4 (0.4)	0.002 (0.002)	1.1 (1.1)
V2	11.8 (1.1)	2.4 (0.08)	15.3 (0.4)
V3	48.8 (14.3)	4.6 (0.03)	5.0 (0.03)
V4	20.8 (0.3)	0.9 (0.0)	0.3 (0.0)
V5	24.1 (8.1)	1.4 (0.2)	8.3 (2.0)
V6	24.1 (8.3)	1.4 (0.2)	8.0 (1.9)
V7	32.4 (9.5)	1.9 (0.3)	10.4 (2.1)
V8	23.3 (7.7)	0.03 (0.004)	0.05 (0.005)
V9	23.4 (8.0)	1.4 (0.2)	16.9 (4.2)
V10	25.6 (8.9)	0.07 (0.03)	0.6 (0.08)
V11	24.2 (6.5)	1.2 (0.2)	29.7 (3.6)
Range	0.4–48.8 (0.4–9.5)	0.002–4.6 (0.0–0.3)	0.05–29.7 (0.0–4.2)

^a Rates are calculated for a synthetic galaxy similar to the Milky Way (solar metallicity, and 10 Gyr of continuous star formation at the level of $3.5 M_{\odot} \text{ yr}^{-1}$). Rates are presented for submodel A (CE HG donor allowed), with the rates for submodel B listed in parentheses (CE HG donor forbidden); see Section 2.3.1 for details. The range presents the minimum and maximum value for each DCO type.

TABLE 3
GALACTIC MERGER RATES, $0.1 Z_{\odot}$ [Myr⁻¹]^a

	NS-NS	BH-NS	BH-BH
S	8.1 (2.5)	3.4 (2.3)	73.3 (13.6)
V1	0.06 (0.06)	0.03 (0.03)	12.5 (8.1)
V2	65.9 (6.9)	0.5 (0.4)	56.7 (16.1)
V3	44.1 (4.2)	15.8 (8.4)	90.2 (7.9)
V4	29.5 (1.4)	8.8 (1.6)	5.9 (0.3)
V5	8.0 (2.3)	3.4 (2.1)	73.4 (13.7)
V6	7.8 (2.4)	3.5 (2.0)	74.5 (13.8)
V7	8.3 (2.2)	6.1 (4.3)	83.7 (15.1)
V8	8.2 (2.5)	0.7 (0.2)	4.2 (0.8)
V9	8.1 (2.1)	5.2 (3.7)	92.3 (19.3)
V10	8.6 (2.6)	2.3 (2.0)	62.0 (11.5)
V11	7.7 (2.3)	3.8 (2.4)	79.2 (17.1)
Range	0.06–65.9 (0.06–6.9)	0.03–15.8 (0.03–8.4)	4.2–92.3 (0.3–19.3)

^aSame as Table 3 but for sub-solar metallicity.

TABLE 4
FORMATION CHANNELS OF DCOs FOR Z_{\odot} ^a

	Channel	Fraction
NSNS01	NC:a→b, SN:a, CE:b→a, NC:b→a, SN:b	79.3%
NSNS02	NC:a→b, CE:b→a, NC:b→a, AIC(WD→NS):a, NC:b→a, SN:b	8.0%
NSNS03	NC:a→b, SN:a, CE:b→a, CE:b→a, ^b SN:b	6.9%
NSNS04	Other	5.8%
BHNS01	NC:a→b, SN:a, CE:b→a, SN:b	95.4%
BHNS02	NC:a→b, SN:a, CE:b→a, NC:b→a, SN:b	1.8%
BHNS03	Other	2.8%
BHBH01	NC:a→b, SN:a, CE:b→a, SN:b	98.9%
BHBH02	Other	1.1%

^a Coalescing DCOs' formation channels for the standard model, submodel A at solar metallicity. NC: non-conservative mass transfer, SN: supernova, CE: common envelope, AIC: accretion induced collapse of oxygen/neon white dwarf into NS. The arrows show the direction of transfer and “a” stands for the primary (initially more massive) component, “b” for the secondary.

^bThe first CE is initiated by the H-rich Hertzsprung gap donor (allowed in model A). The second starts when the exposed core of the donor becomes an evolved helium star.

TABLE 5
FORMATION CHANNELS OF DCOs FOR 0.1 Z_{\odot} ^a

	Channel	Fraction
NSNS01	NC:a→b, SN:a, CE:b→a, CE:b→a, SN:b	49.1%
NSNS02	NC:a→b, SN:a, CE:b→a, NC:b→a, SN:b	21.2%
NSNS03	NC:a→b, SN:a, CE:b→a, SN:b	18.2%
NSNS04	NC:a→b, CE:b→a, SN:a, CE:b→a, SN:b	3.3%
NSNS05	Other	8.2%
BHNS01	CE:a→b, SN:a, CE:b→a, NC:b→a, SN:b	40.8%
BHNS02	CE:a→b, SN:a, CE:b→a, SN:b	17.4%
BHNS03	NC:a→b, SN:a, CE:b→a, SN:b	13.4%
BHNS04	NC:a→b, SN:a, CE:b→a, NC:b→a, SN:b	12.2%
BHNS05	NC:a→b, CE:b→a, NC:a→b, SN:a, SN:b	8.8%
BHNS06	Other	6.4%
BHBH01	NC:a→b, SN:a, CE:b→a, SN:b	90.6%
BHBH02	CE:a→b, SN:a, CE:b→a, SN:b	4.0%
BHBH03	NC:a→b, SN:a, NC:b→a, CE:b→a, SN:b	1.4%
BHBH04	Other	4.0%

^a Same as Table 4 but for sub-solar metallicity.

TABLE 6
CHIRP MASS CHARACTERISTICS FOR Z_{\odot} , SUBMODEL A^a

	NS-NS			BH-NS			BH-BH		
	min	avg	max	min	avg	max	min	avg	max
S	0.96	1.05	1.40	2.3	3.2	3.7	5.1	6.7	8.7
V1	1.08	1.09	1.14	3.2	3.2	3.2	5.3	6.5	8.3
V2	0.96	1.08	1.53	2.5	3.2	4.0	5.0	6.6	8.4
V3	0.94	1.06	1.69	2.1	2.7	3.6	4.9	6.0	7.7
V4	0.95	1.03	1.64	2.1	2.5	3.1	5.0	5.8	6.3
V5	0.96	1.05	1.42	2.4	3.2	3.8	5.0	6.7	8.7
V6	0.96	1.05	1.44	2.2	3.2	3.9	3.5	6.7	8.8
V7	0.96	1.05	1.45	2.1	3.1	3.9	5.0	6.5	8.7
V8	0.96	1.05	1.42	2.6	3.0	3.2	5.4	6.5	7.4
V9	0.96	1.05	1.44	2.2	3.1	3.7	5.0	6.3	7.5
V10	1.01	1.14	1.86	2.0	3.1	4.2	2.7	5.7	7.6
V11	0.96	1.05	1.50	2.7	3.2	4.2	4.9	10.5	14.3
Range	0.94–1.86			2.0–4.2			2.7–14.3		

^a The chirp mass distribution for merging DCOs, for Z_{\odot} and submodel A. The values of chirp mass presented are: minimum, average, and maximum in units of M_{\odot} . The range represents the minimum–maximum value of the chirp mass from the entire suite of models for each DCO type. This table corresponds to Fig. 10.

TABLE 7
CHIRP MASS CHARACTERISTICS FOR Z_{\odot} , SUBMODEL B^a

	NS-NS			BH-NS			BH-BH		
	min	avg	max	min	avg	max	min	avg	max
S	0.96	1.05	1.17	2.3	3.2	3.3	5.2	6.7	7.4
V1	1.08	1.09	1.14	3.2	3.2	3.2	5.3	6.5	8.3
V2	0.96	1.06	1.53	3.0	3.2	3.3	5.6	6.5	7.2
V3	0.96	1.05	1.22	2.2	2.4	2.6	5.7	5.9	6.4
V4	1.03	1.03	1.04	no systems			no systems		
V5	0.96	1.05	1.28	2.4	3.1	3.3	5.2	6.7	7.4
V6	0.96	1.05	1.43	2.6	3.2	3.4	3.5	6.7	8.7
V7	0.96	1.05	1.45	2.2	3.1	3.5	5.1	6.5	8.0
V8	0.96	1.05	1.08	3.2	3.2	3.2	5.6	5.9	6.1
V9	0.96	1.05	1.21	2.2	3.1	3.3	5.0	6.2	7.4
V10	1.04	1.13	1.34	2.0	3.0	4.2	2.7	4.6	6.6
V11	0.96	1.05	1.09	2.9	3.3	4.0	4.9	9.1	13.8
Range	0.96–1.53			2.0–4.2			2.7–13.8		

^a Same as Table 6 but for submodel B. This table corresponds to Fig. 11.

TABLE 8
CHIRP MASS CHARACTERISTICS FOR $0.1 Z_{\odot}$, SUBMODEL A^a

	NS-NS			BH-NS			BH-BH		
	min	avg	max	min	avg	max	min	avg	max
S	0.96	1.09	1.67	2.1	3.2	6.1	4.8	13.2	31.8
V1	1.08	1.11	1.56	2.9	3.6	4.4	5.9	20.0	32.3
V2	0.96	1.09	1.66	2.3	3.5	6.5	4.8	17.2	31.6
V3	0.96	1.09	1.68	2.0	2.9	6.1	4.8	12.5	29.7
V4	0.95	1.10	1.64	2.1	2.9	5.9	4.8	7.6	28.1
V5	0.96	1.09	1.66	2.0	3.1	4.6	4.8	13.3	31.8
V6	0.97	1.09	1.65	1.7	3.1	5.2	4.8	13.1	31.8
V7	0.96	1.08	1.70	2.0	3.1	6.4	4.9	12.4	32.0
V8	0.96	1.09	1.64	2.0	3.0	6.4	4.8	9.0	31.9
V9	0.97	1.08	1.66	2.0	3.0	6.1	4.9	12.1	31.9
V10	1.10	1.20	2.16	1.8	3.4	6.3	2.4	14.4	32.0
V11	0.97	1.08	1.61	2.0	3.3	4.7	4.8	14.3	41.4
Range	0.95–2.16			1.7–6.4			2.4–41.4		

^a Same as Table 6 but for $0.1 Z_{\odot}$. This table corresponds to Fig. 12.

TABLE 9
CHIRP MASS CHARACTERISTICS FOR $0.1 Z_{\odot}$, SUBMODEL B^a

	NS-NS			BH-NS			BH-BH		
	min	avg	max	min	avg	max	min	avg	max
S	0.96	1.09	1.67	2.2	3.1	4.6	4.8	9.7	18.3
V1	1.08	1.11	1.56	2.9	3.6	4.4	5.9	16.1	32.3
V2	0.96	1.07	1.66	2.3	3.3	4.6	4.8	9.3	18.8
V3	0.99	1.12	1.68	2.0	2.9	4.5	4.8	6.8	14.9
V4	0.98	1.20	1.60	2.1	2.7	3.6	5.0	6.7	11.5
V5	0.96	1.08	1.66	2.2	3.2	4.6	4.8	9.8	17.7
V6	0.98	1.09	1.65	1.7	3.2	4.6	4.8	9.7	18.3
V7	0.96	1.08	1.60	2.1	3.1	4.6	4.9	9.7	17.7
V8	0.96	1.09	1.64	2.2	3.0	4.4	4.8	7.2	16.3
V9	0.98	1.08	1.55	2.1	3.0	4.5	4.9	9.3	18.1
V10	1.10	1.20	2.13	2.0	3.4	5.0	2.4	10.2	17.5
V11	0.97	1.08	1.61	2.3	3.4	4.7	4.8	10.6	19.1
Range	0.96–2.13			1.7–5.0			2.4–32.3		

^a Same as Table 8 but for submodel A. This table corresponds to Fig. 13.

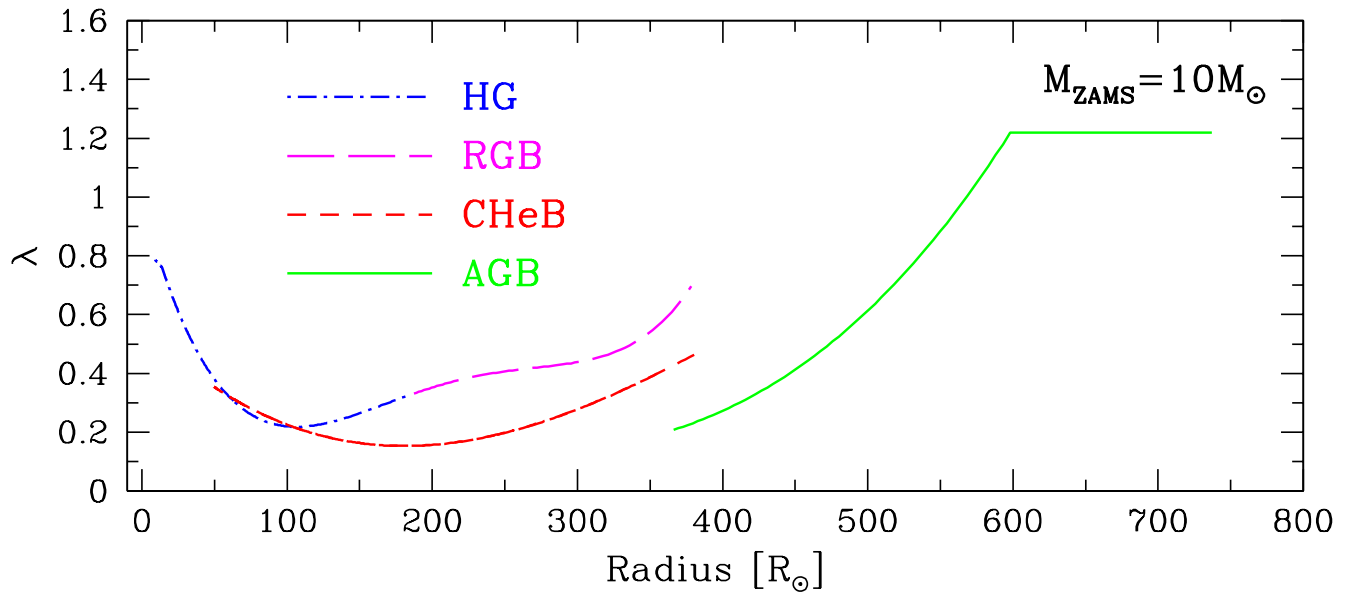


Fig. 1.— The binding energy parameter, λ , as a function of stellar radius, presented in Xu & Li (2010) (*Nanjing* λ) for a typical NS progenitor in a NS-NS system ($M_{\text{ZAMS}} = 10 M_{\odot}$) at Z_{\odot} . HG stands for Hertzsprung Gap, RGB for Red Giant Branch, CHeB for Core Helium Burning, and AGB for Asymptotic Giant Branch. The general behaviour of λ is described in Section 2.3.

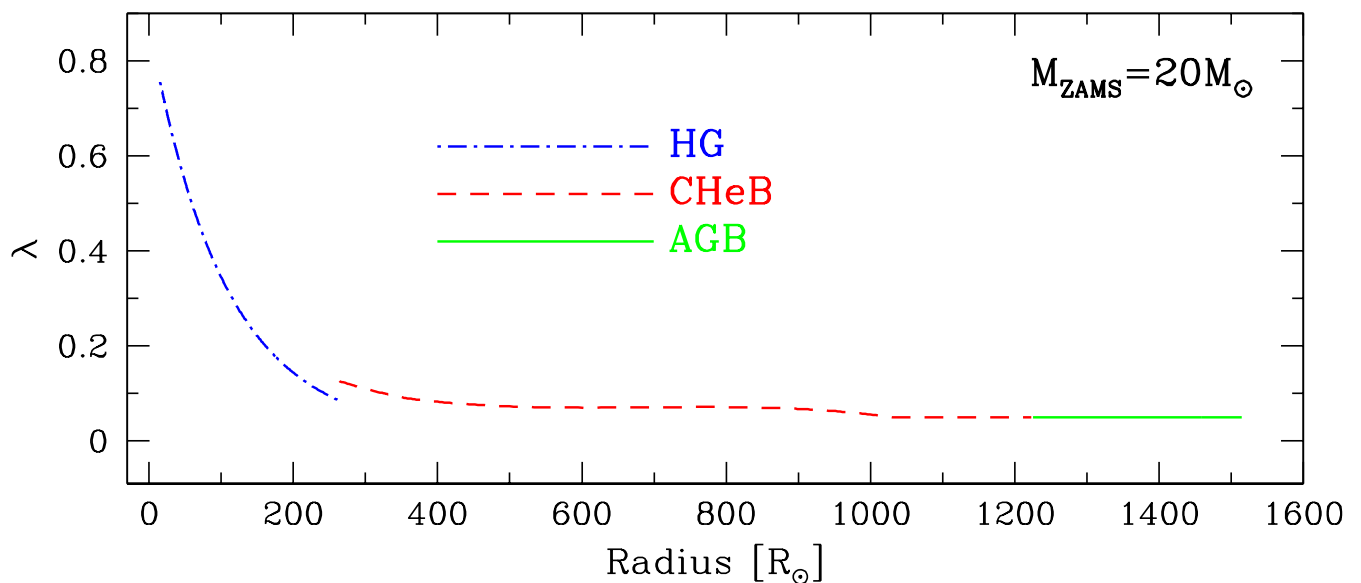


Fig. 2.— The same as Fig. 1 but for a BH-NS system ($M_{\text{ZAMS}} = 20 M_{\odot}$).

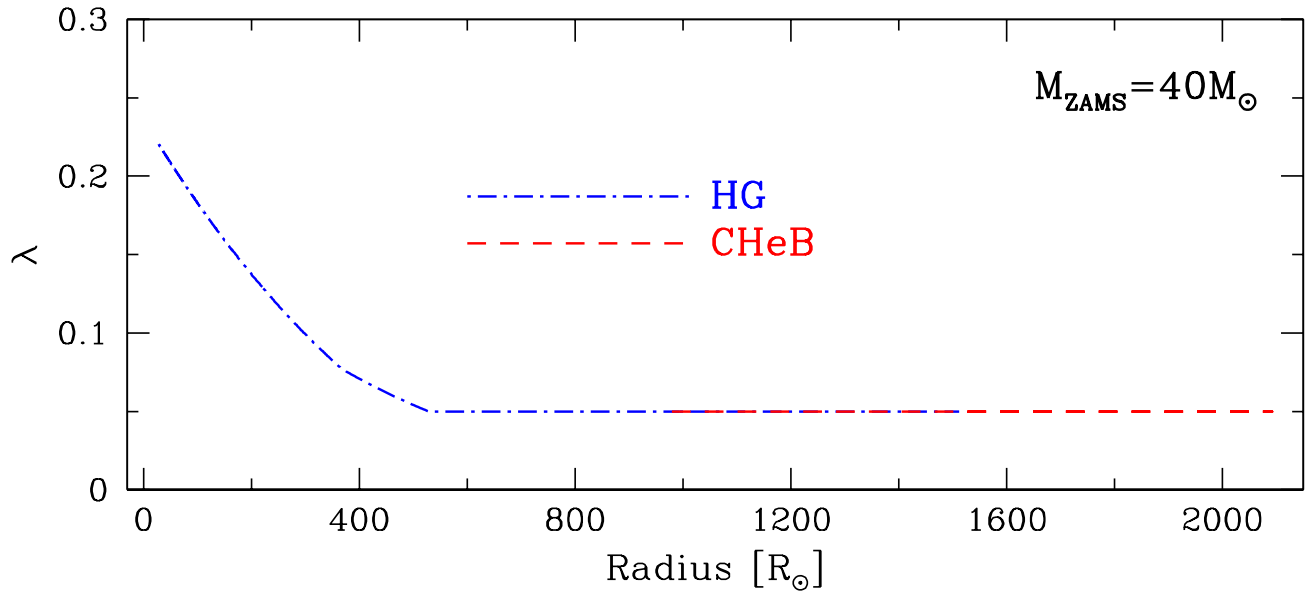


Fig. 3.— *Nanjing* λ of a typical progenitor for the secondary component in a BH-BH system ($M_{\text{ZAMS}} = 40 M_{\odot}$) at solar metallicity.

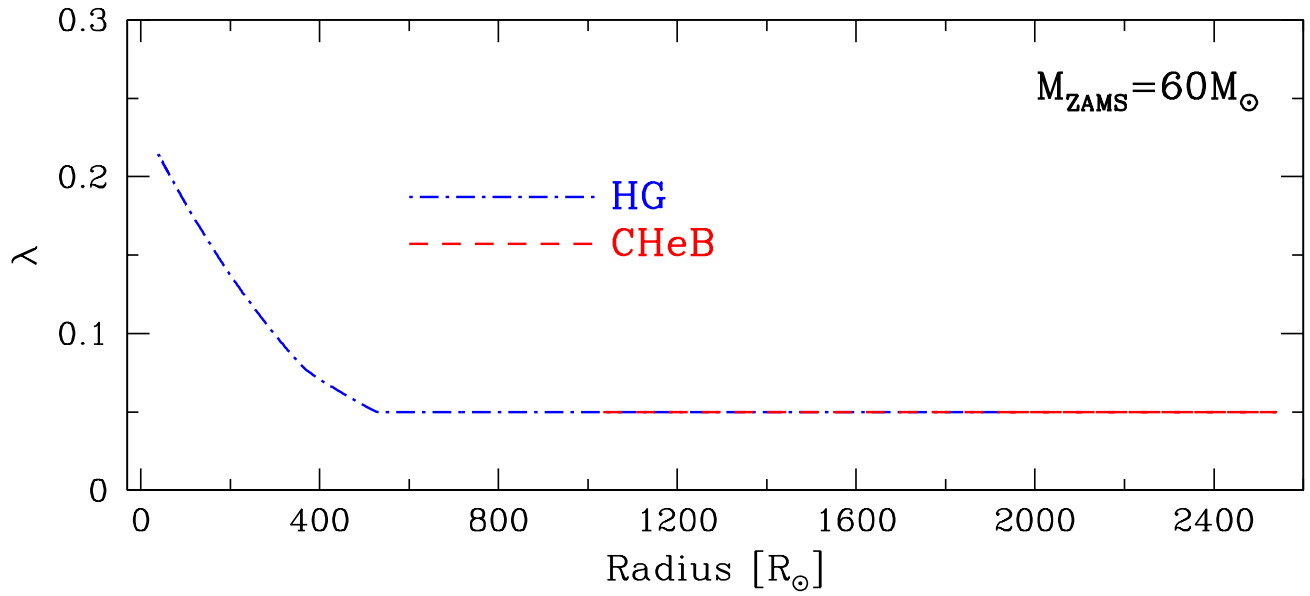


Fig. 4.— Same as Fig. 3 but for the progenitor of the primary component.

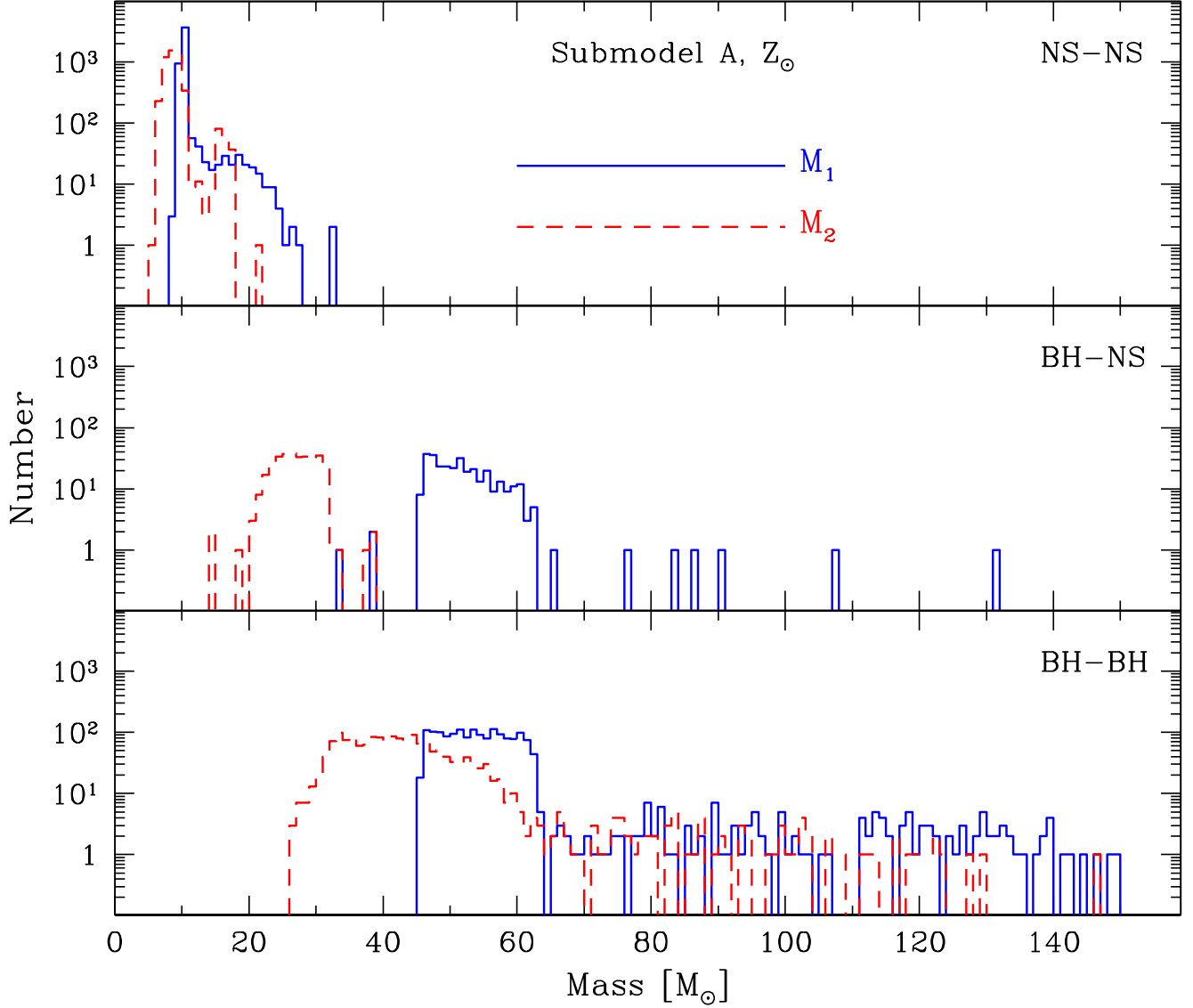


Fig. 5.— The distribution of progenitor (ZAMS) masses of coalescing DCOs for the standard model, submodel A, Z_{\odot} . The top panel presents the distribution for NS-NS, the middle panel for BH-NS, and the bottom panel for BH-BH progenitors. M_1 stands for the primary component (initially more massive, solid, blue line) and M_2 for the secondary (initially less massive, dashed, red line). The average mass for NS-NS progenitors is 11–9 M_{\odot} , for BH-NS progenitors 52–27 M_{\odot} , and for BH-BH progenitors 58–44 M_{\odot} (M_1 – M_2). Note that binary evolution blurs the ZAMS mass limits for NS/BH formation (see Section 4.1).

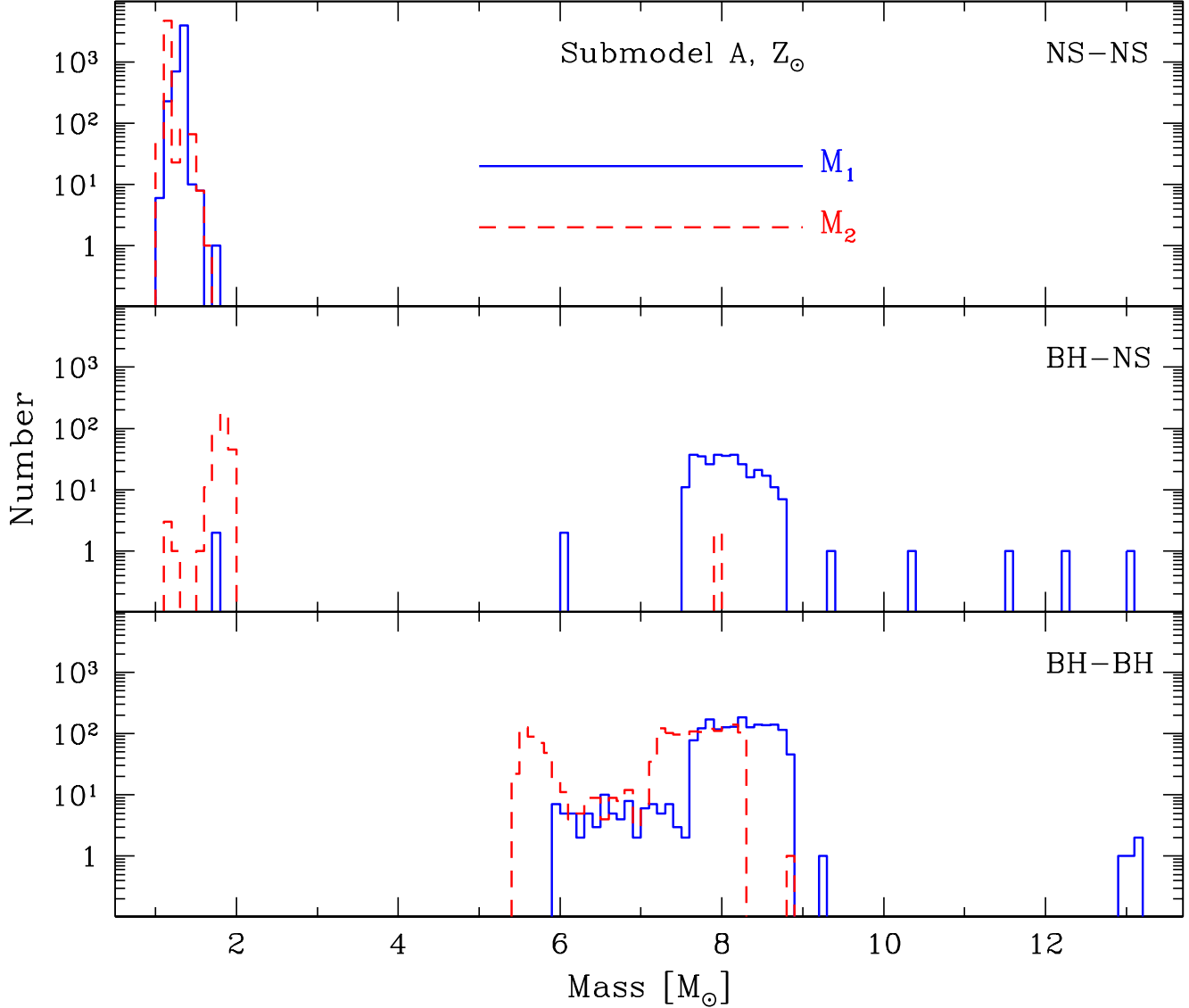


Fig. 6.— The distribution of remnant masses of coalescing DCOs for the standard model, submodel A, Z_{\odot} . The top panel presents the distribution for NS-NS, the middle panel for BH-NS, and the bottom panel for BH-BH systems. M_1 represents the primary remnant (corresponding to M_1 in Fig. 5, solid, blue line) while M_2 is the secondary (corresponding to M_2 in Fig. 5, dashed, red line). The average mass for NS-NS systems is $1.3\text{--}1.1 M_{\odot}$, for BH-NS systems $8.0\text{--}1.8 M_{\odot}$, and for BH-BH systems $8.2\text{--}7.2 M_{\odot}$ ($M_1\text{--}M_2$). The gap between the upper mass of NSs ($2 M_{\odot}$) and the lowest mass of BHs ($5 M_{\odot}$) results from the use of the Rapid SN engine (see Section 2.4).

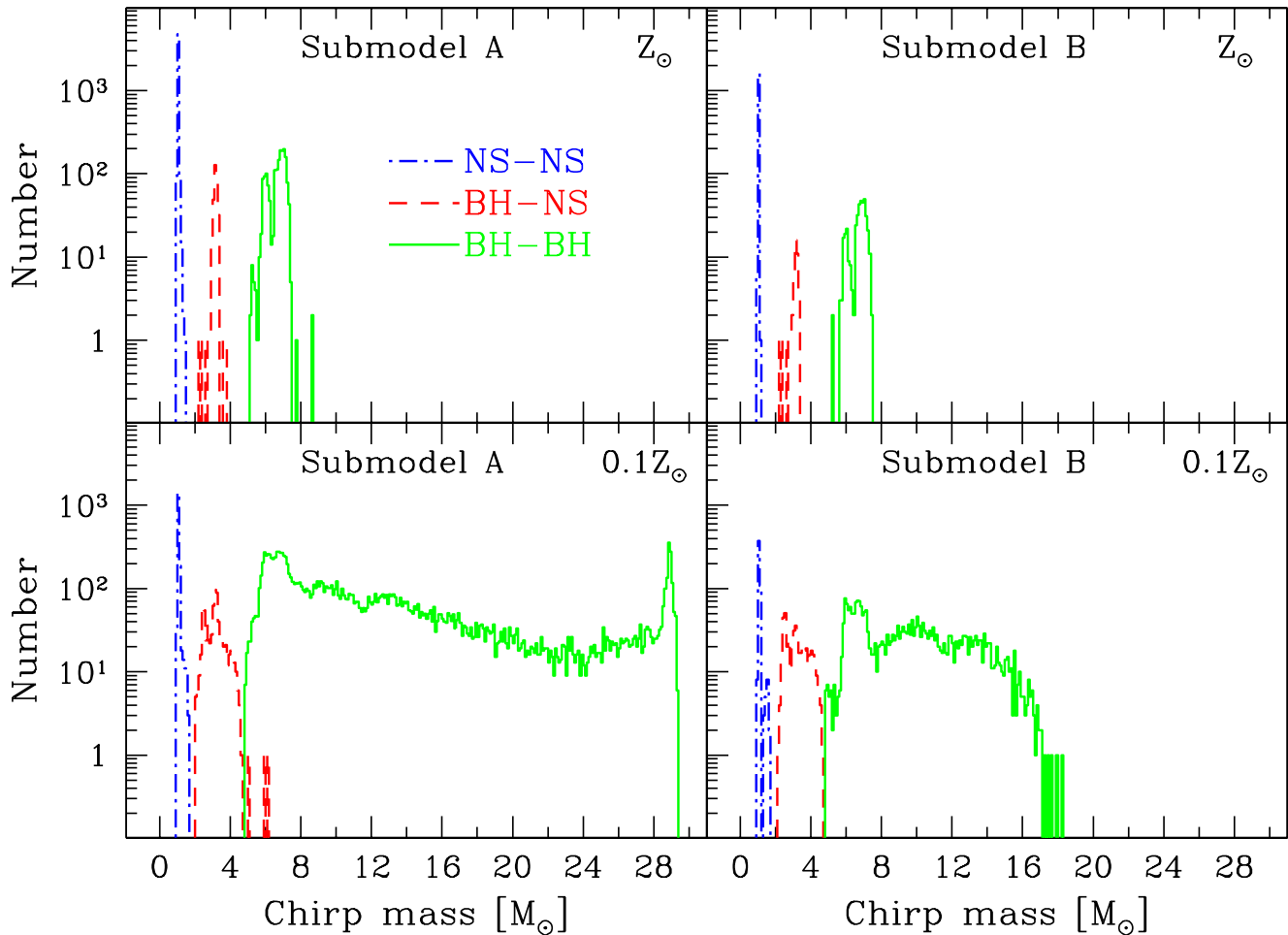


Fig. 7.— The distribution of chirp masses of coalescing DCOs for the standard model. The average chirp masses for NS-NS and BH-NS systems are $\sim 1.1 M_{\odot}$ and $3.2 M_{\odot}$, respectively, for both submodels and metallicities. The average chirp mass for BH-BH systems, for Z_{\odot} , is $\sim 6.7 M_{\odot}$ for both submodels. For $0.1 Z_{\odot}$ the masses are $13.2\text{--}9.7 M_{\odot}$ for submodel A and B, respectively. The maximum chirp mass increases with metallicity as wind mass loss rates decrease, allowing for the formation of heavier BHs (see Belczynski et al. (2010b) and Section 4.1).

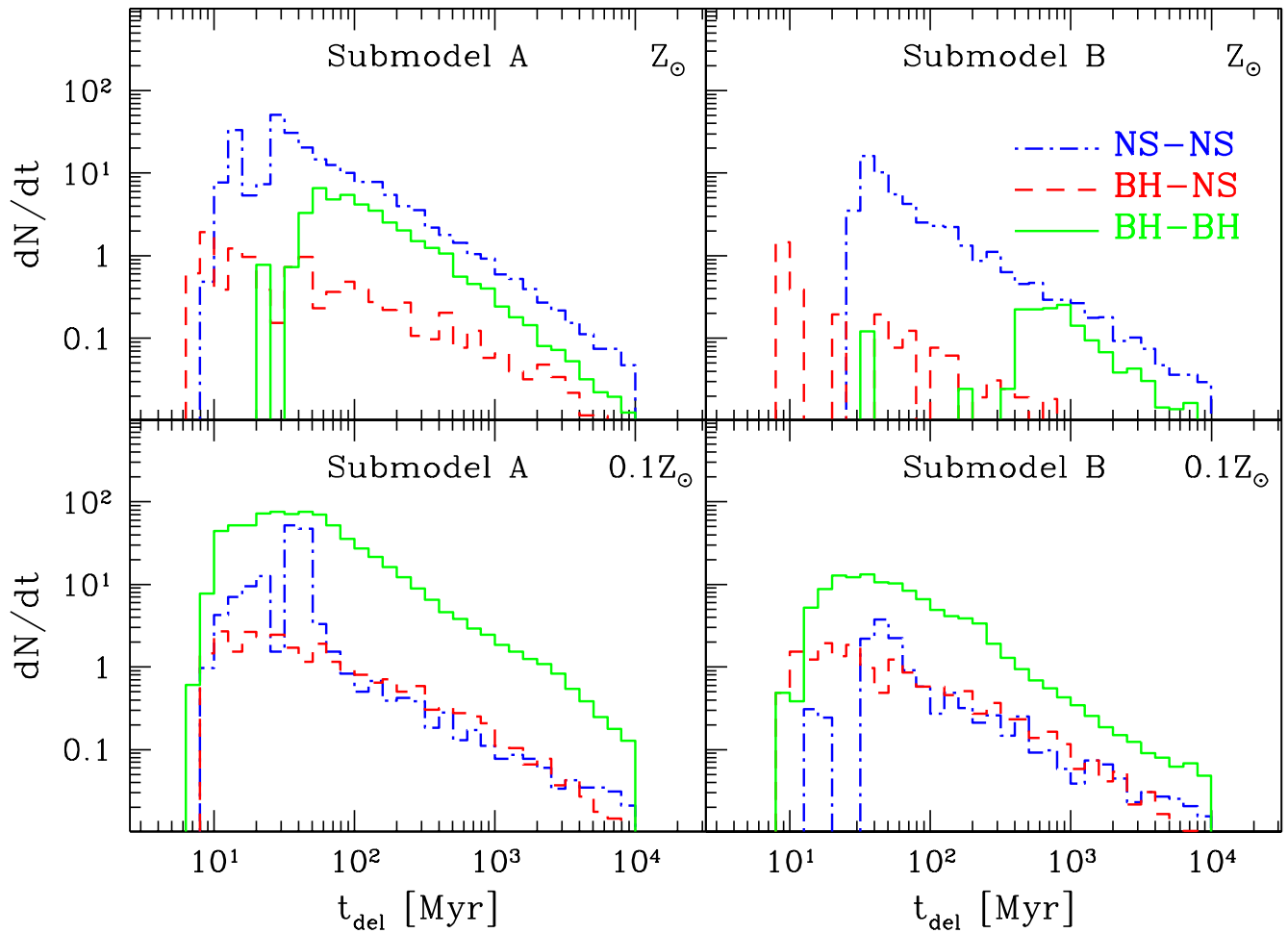


Fig. 8.— The distribution of delay times for coalescing DCOs, for the standard model. The vertical axis present the number of DCOs per linear time. The average delay time for all binaries is ~ 1 Gyr.

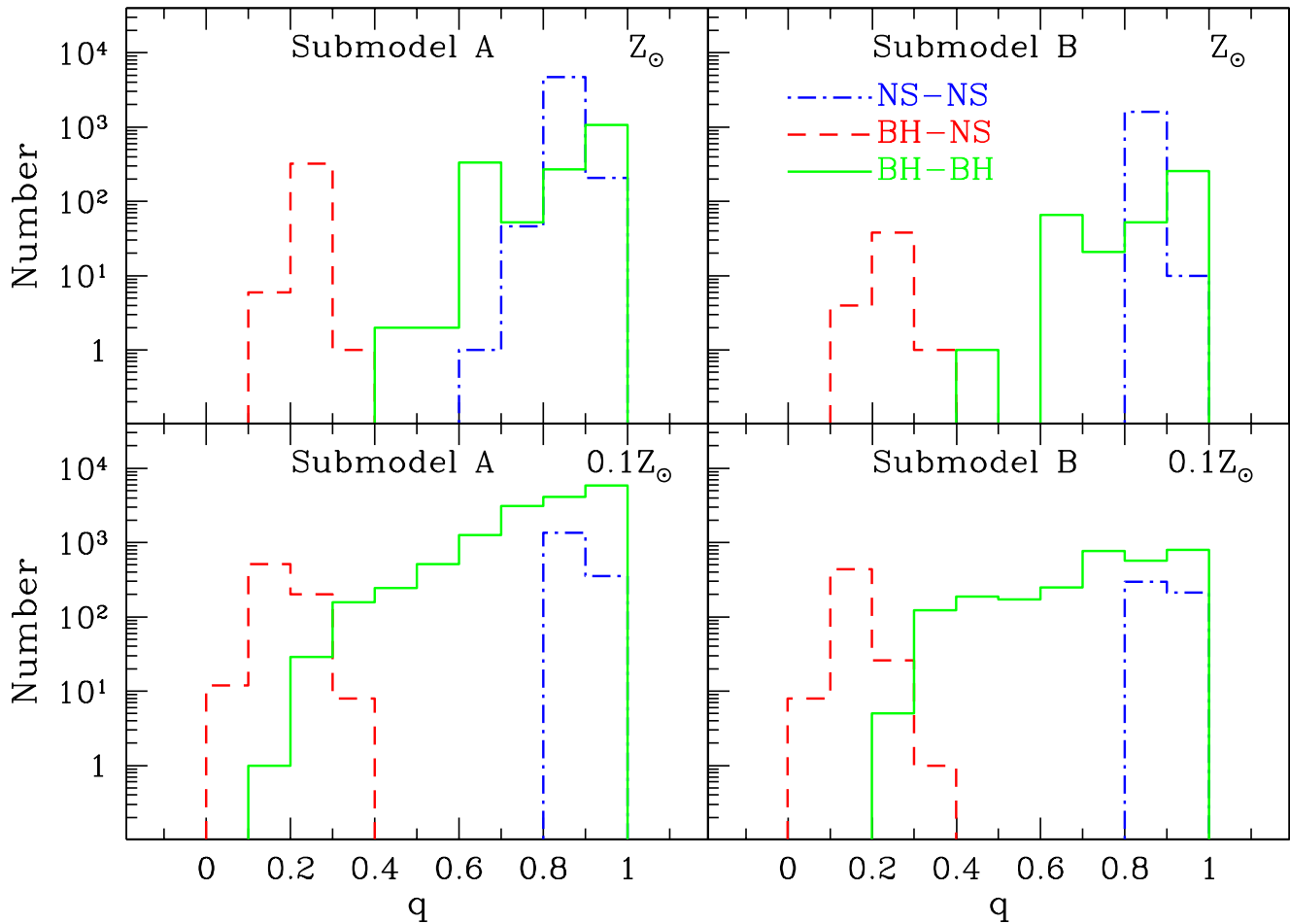


Fig. 9.— The distribution of mass ratios of coalescing DCOs for the standard model. The mass ratio is defined as the ratio of the less massive to the more massive compact object in the binary. The average values for NS-NS systems are ~ 0.85 for both submodels and metallicities. For BH-NS binaries the average is ~ 0.22 for Z_{\odot} , for both submodels and ~ 0.15 for $0.1 Z_{\odot}$, also for both submodels. For BH-BH systems the average value is ~ 0.8 for both submodels and metallicities.

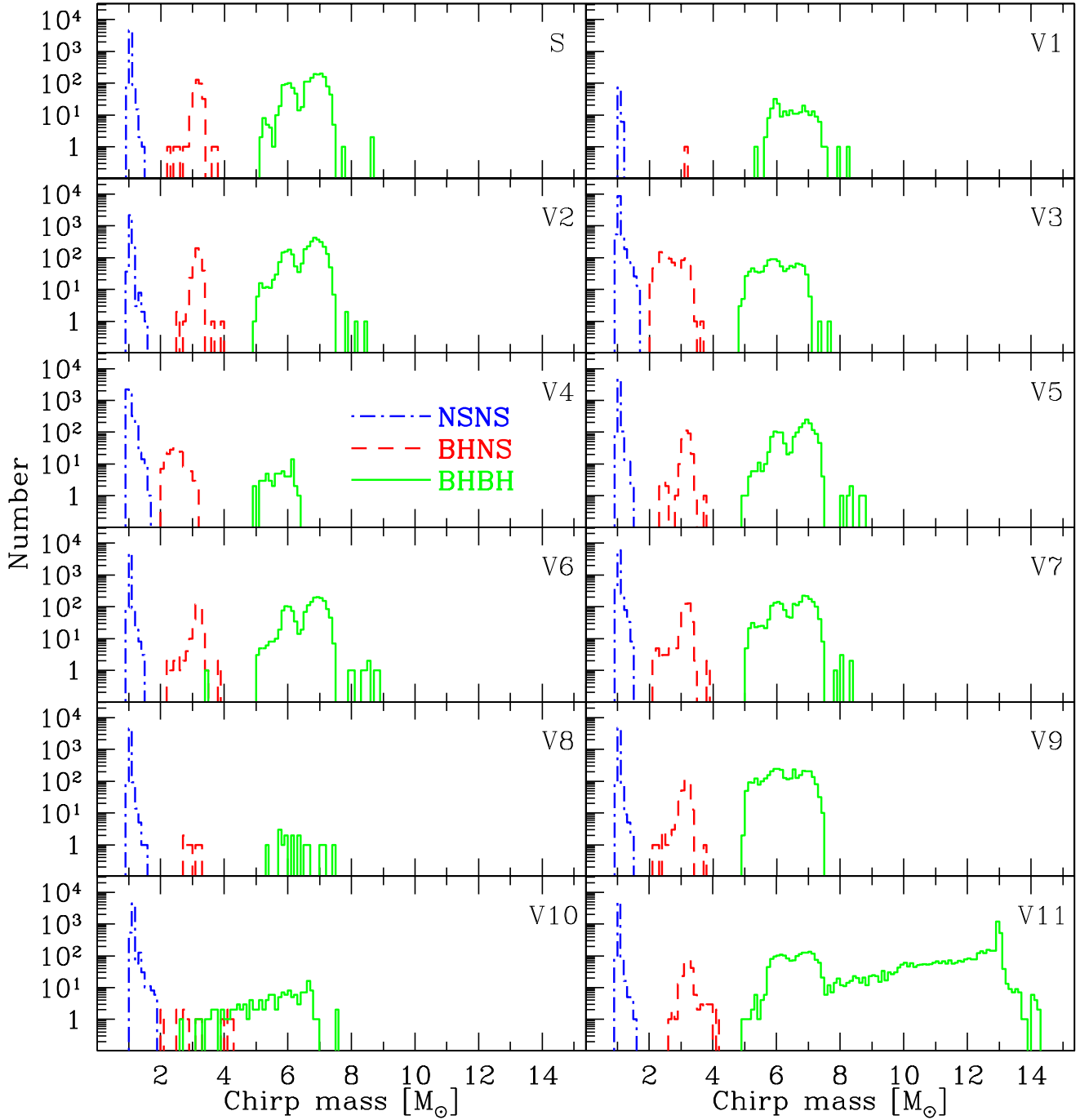


Fig. 10.— The chirp mass distribution of coalescing double compact objects for all variations for submodel A and $Z = Z_{\odot}$. The maximum chirp mass is found for BH-BH systems, and may reach as high as $\sim 14 M_{\odot}$. The typical chirp mass for BH-NS systems is $\sim 2-3 M_{\odot}$, while the chirp mass for NS-NS systems peaks around $\sim 1 M_{\odot}$ independent of the model. Note that the chirp masses of BH-NS systems are separated from the BH-BH values. The only exception to this rule is the (most-likely unphysical) V10 model, which employs the Delayed supernova engine (see Sec. 4.10 for details).

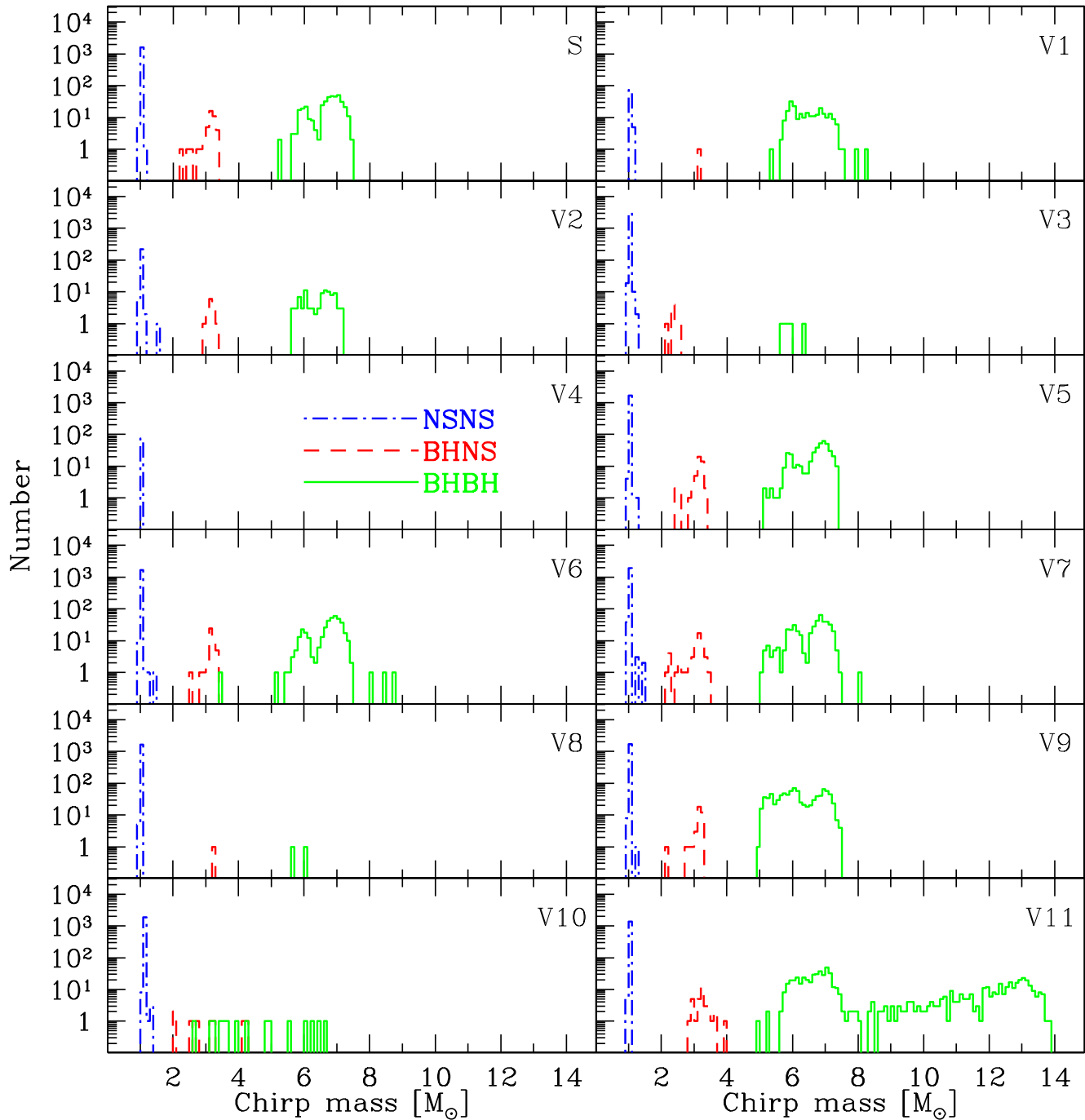


Fig. 11.— The chirp mass distribution of coalescing double compact objects for all variations for submodel B and $Z = Z_{\odot}$.

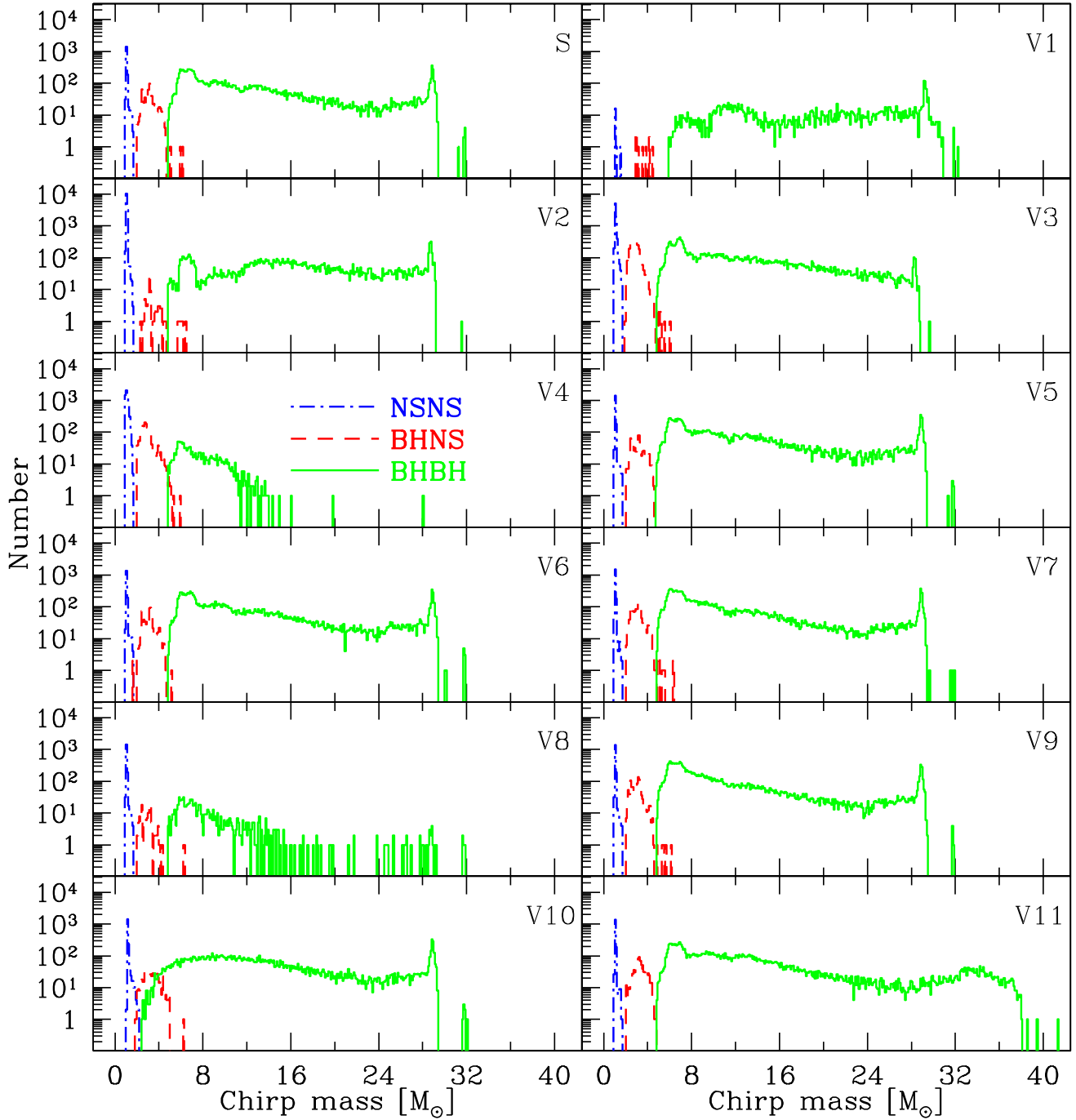


Fig. 12.— The chirp mass distribution of coalescing double compact objects for all variations for submodel A and $Z = 0.1 Z_\odot$. Note the dramatic increase of the maximum chirp mass with decreasing metallicity. For solar metallicity, the chirp mass was always below $10 M_\odot$ (Fig. 10), while for the majority of models shown here, the chirp mass reaches $\sim 30 M_\odot$ for sub-solar metallicity. The lack of high chirp-mass systems in model V4 is explained in Sec. 4.5.

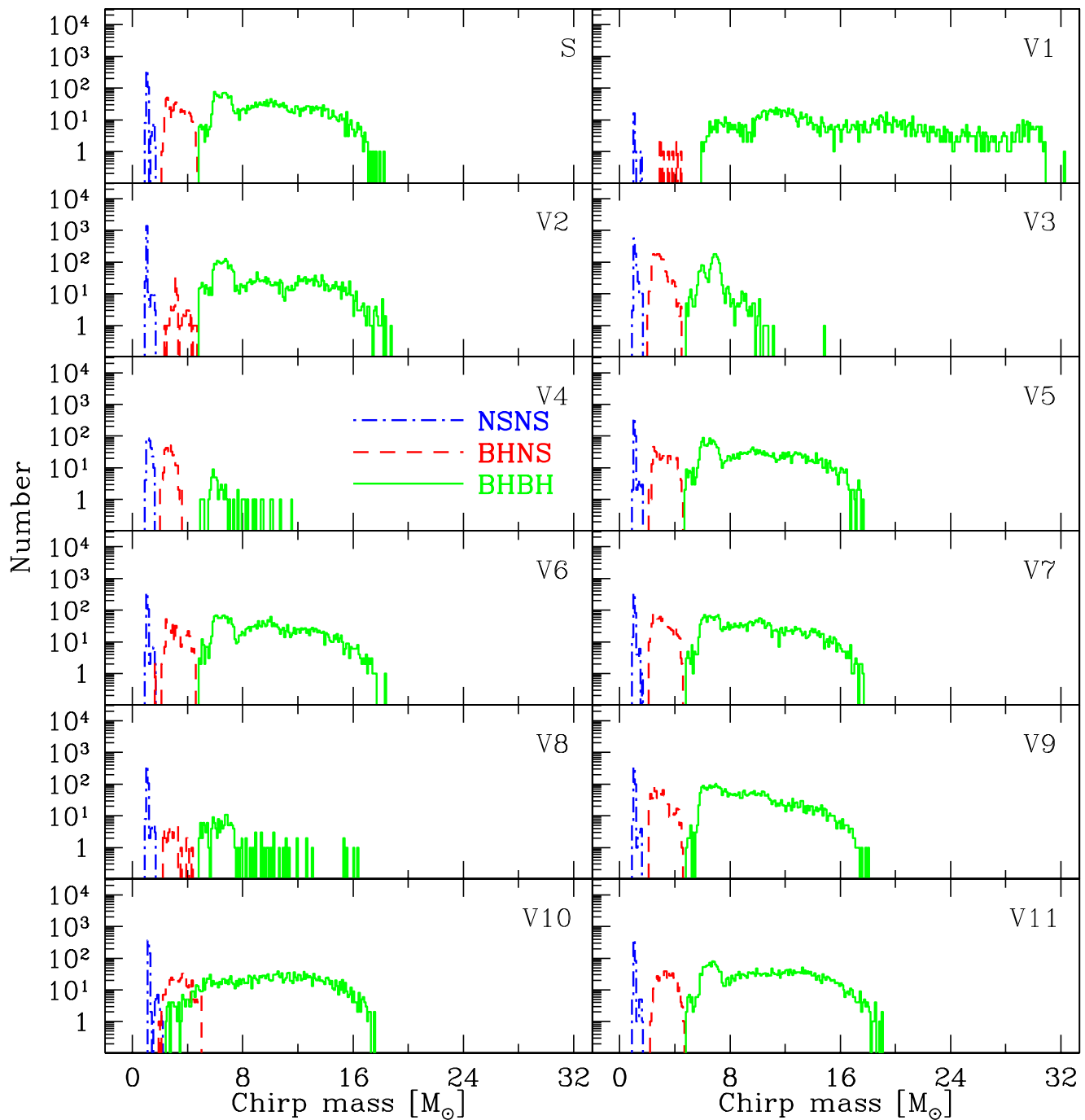


Fig. 13.— The chirp mass distribution of coalescing double compact objects for all variations for submodel B and $Z = 0.1 Z_{\odot}$. The maximum chirp mass for submodel B typically reaches only $\sim 15 M_{\odot}$, as contrasted with $\sim 30 M_{\odot}$ for submodel A (see Fig. 12). The reason why the V1 model allows for chirp mass as high as $\sim 30 M_{\odot}$, even for submodel B, is explained in Sec. 4.2.

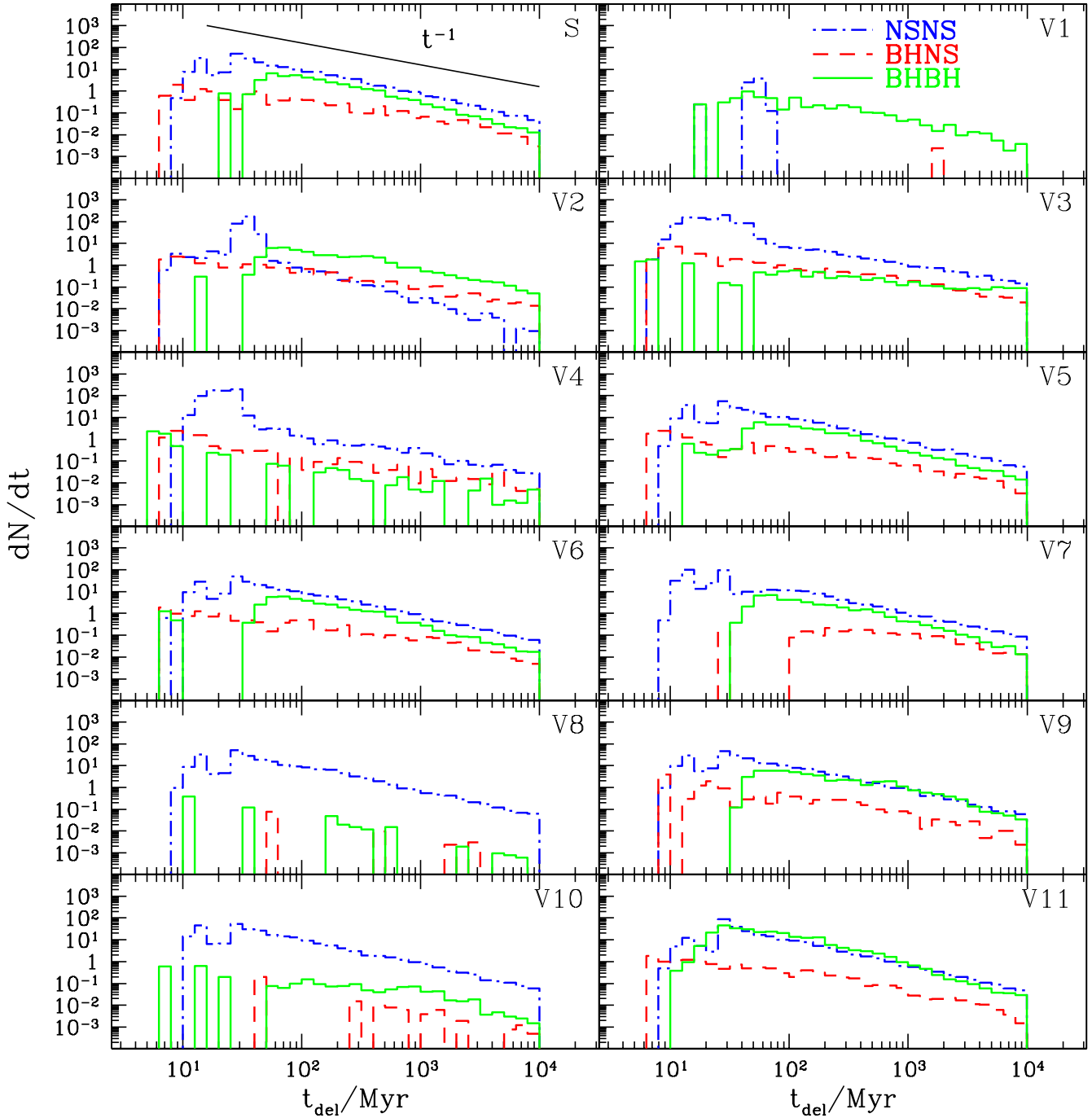


Fig. 14.— The delay time distribution of coalescing double compact objects for all variations for submodel A and $Z = Z_{\odot}$. Note that especially at later times the number of sources typically falls off as $\propto t_{\text{del}}^{-1}$.

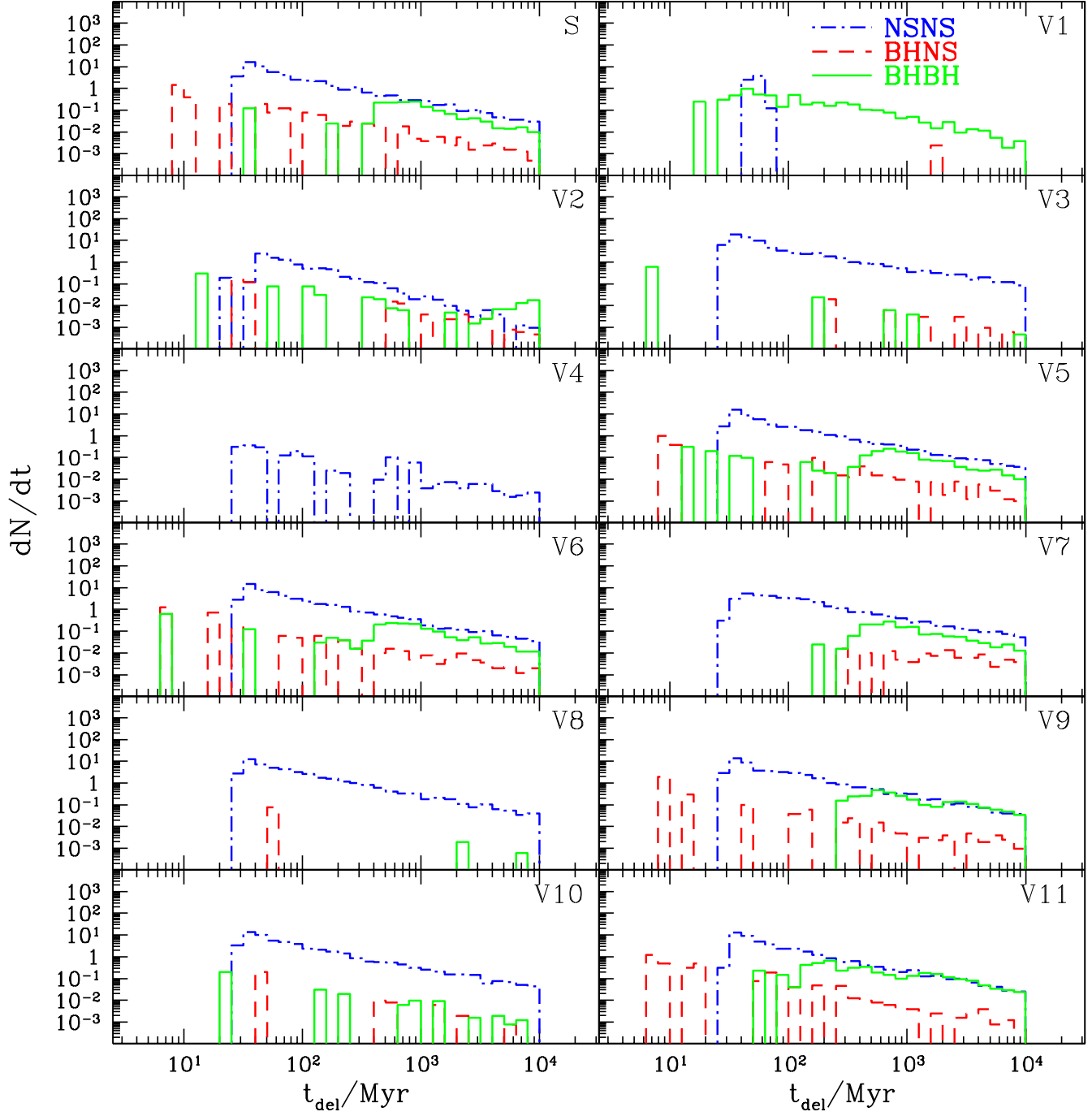


Fig. 15.— Same as Fig. 14 but for submodel B.

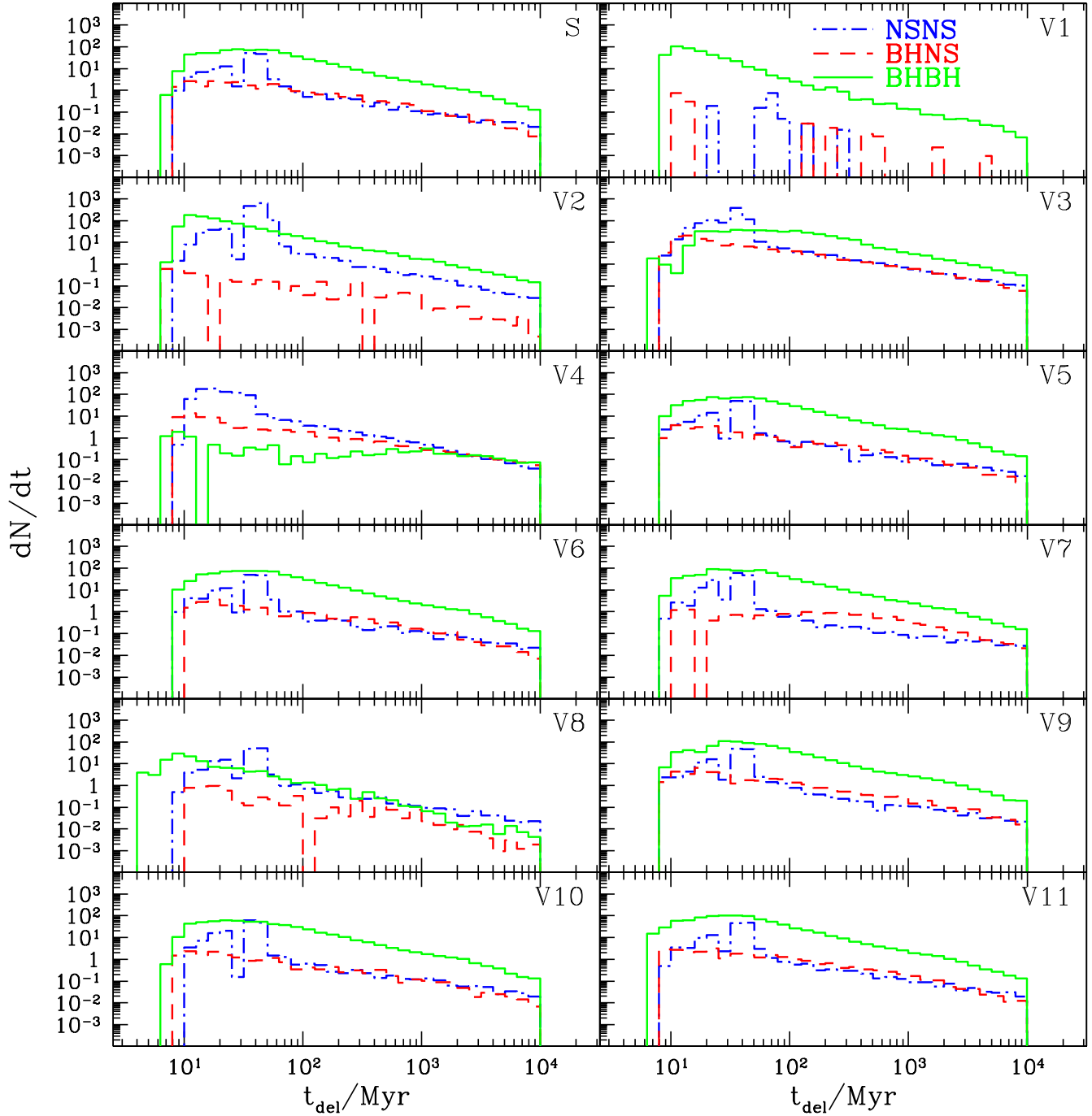


Fig. 16.— Same as Fig. 14 but for $0.1 Z_{\odot}$. The average delay time for systems containing BHs decreases with decreasing metallicity as the components become more massive.

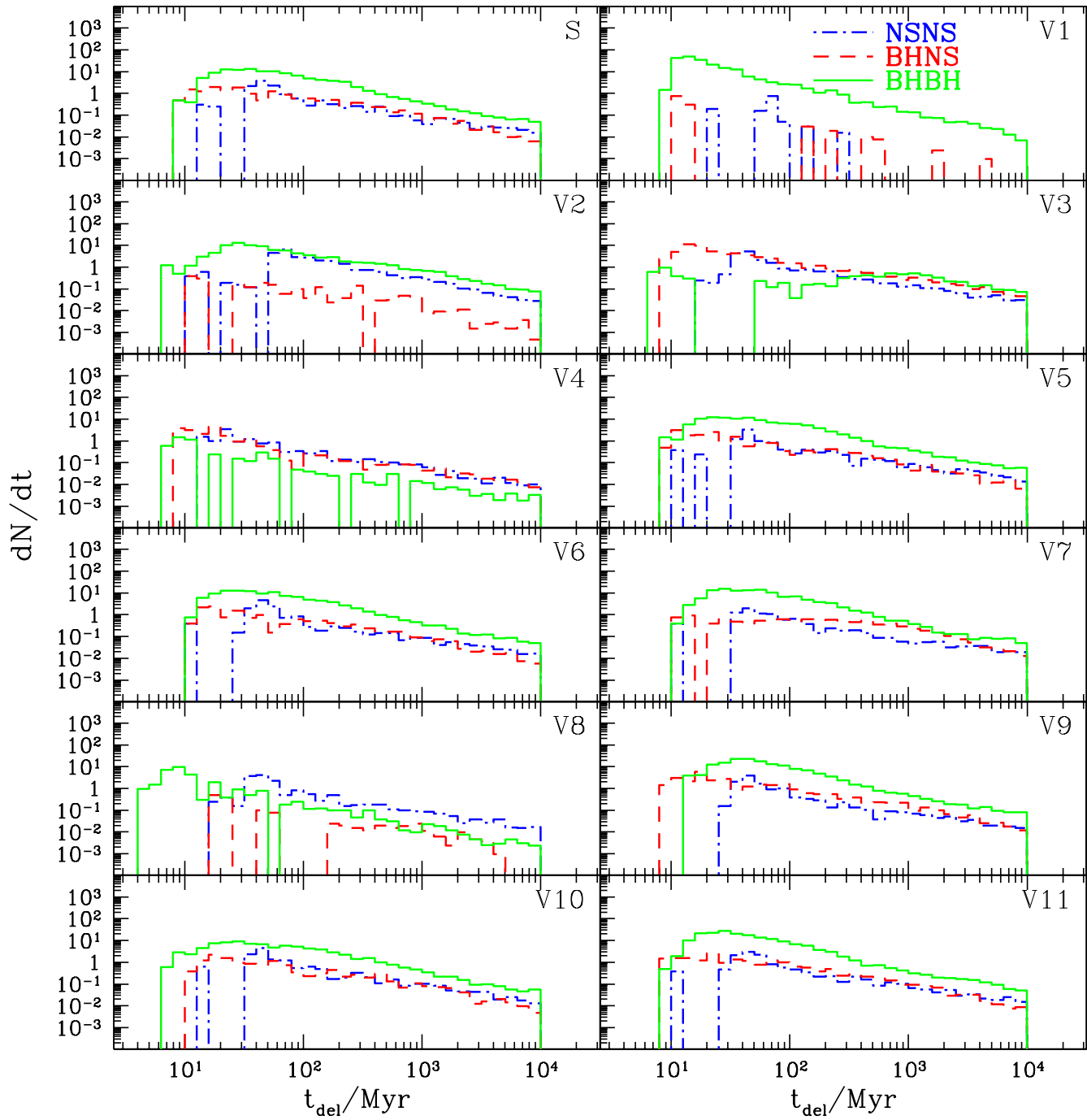


Fig. 17.— Same as Fig. 16 but for submodel B.

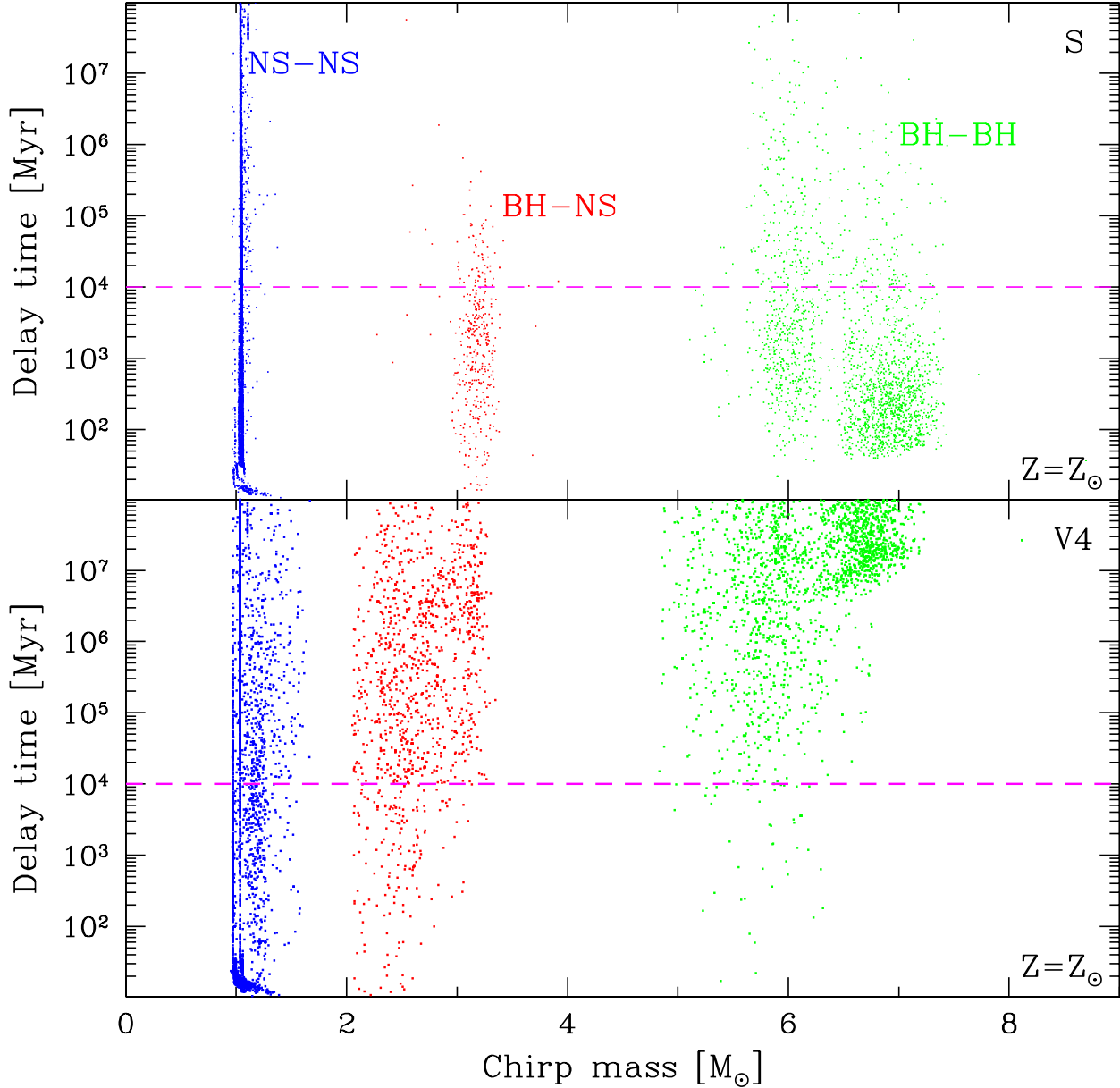


Fig. 18.— Chirp mass—delay time diagrams for merging DCOs for submodel A, $Z = Z_{\odot}$. *Top panel.* Results for the standard model. Significant populations of DCOs containing BHs are present below the 10 Gyr delay time limit (the horizontal dashed magenta line). *Bottom panel.* Results for V4. Weakly bound envelopes, represented by a very high λ value, cause insignificant separation reduction during the CE phase. This results in only a few systems crossing the 10 Gyr time limit and into the merging population. Both of these panels illustrate the migration of DCOs between the merging and non-merging populations with varying λ values. The clustering of chirp masses around higher values for merging DCOs with BHs in the standard model comes from the fact that more massive progenitors are more likely to survive a strongly bound CE phase due to a larger orbital energy reservoir. Note that these diagrams do not show the full range of the non-merging populations; systems with delay times much larger than 10^8 Myr and masses larger than $8 M_{\odot}$ may also be formed.

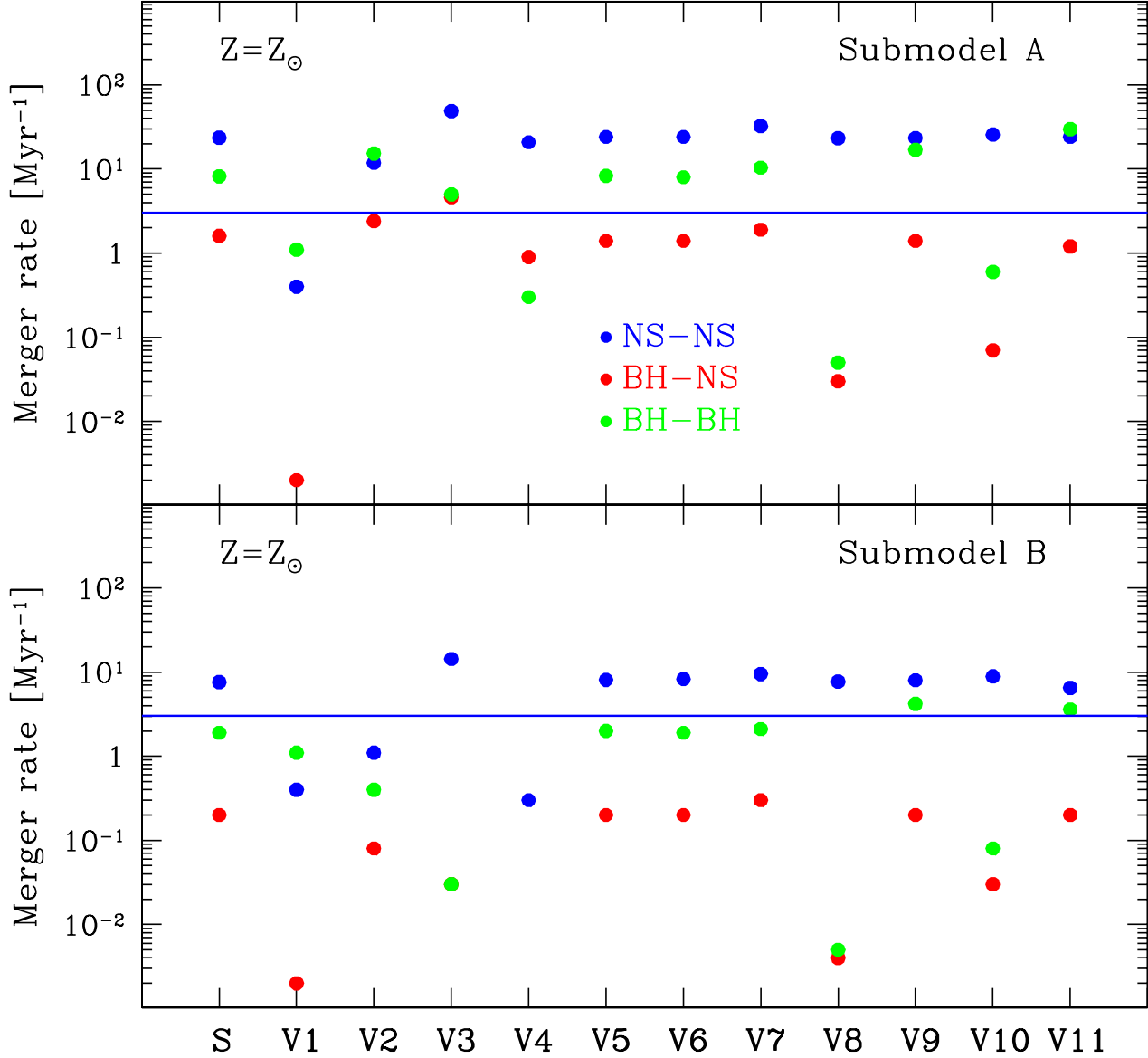


Fig. 19.— Galactic merger rates from all of our models, with submodel A in the top panel and B in the bottom, for $Z = Z_{\odot}$. The blue solid line represents the lower limit for predicted merger rates of NS-NS systems observed in our Galaxy (at 3 Myr^{-1}) as shown in Kim et al. (2006). Models yielding merger rates of NS-NS systems lower than this value are disfavored; these are V1-submodel A, V1-submodel B, V2-submodel B, V4-submodel B. *Reminder:* the described models are: V1–V4, changing λ from 0.01 to 10; V5–V6, changing $M_{\text{NS,max}}$ from $3.0 M_{\odot}$ to $2.5 M_{\odot}$; V7 – reducing natal kicks for all DCOs, V8–V9, full and no natal kicks for BHs, respectively; V10 – investigating the Delayed SN engine; V11 – reducing wind mass loss rates by half.

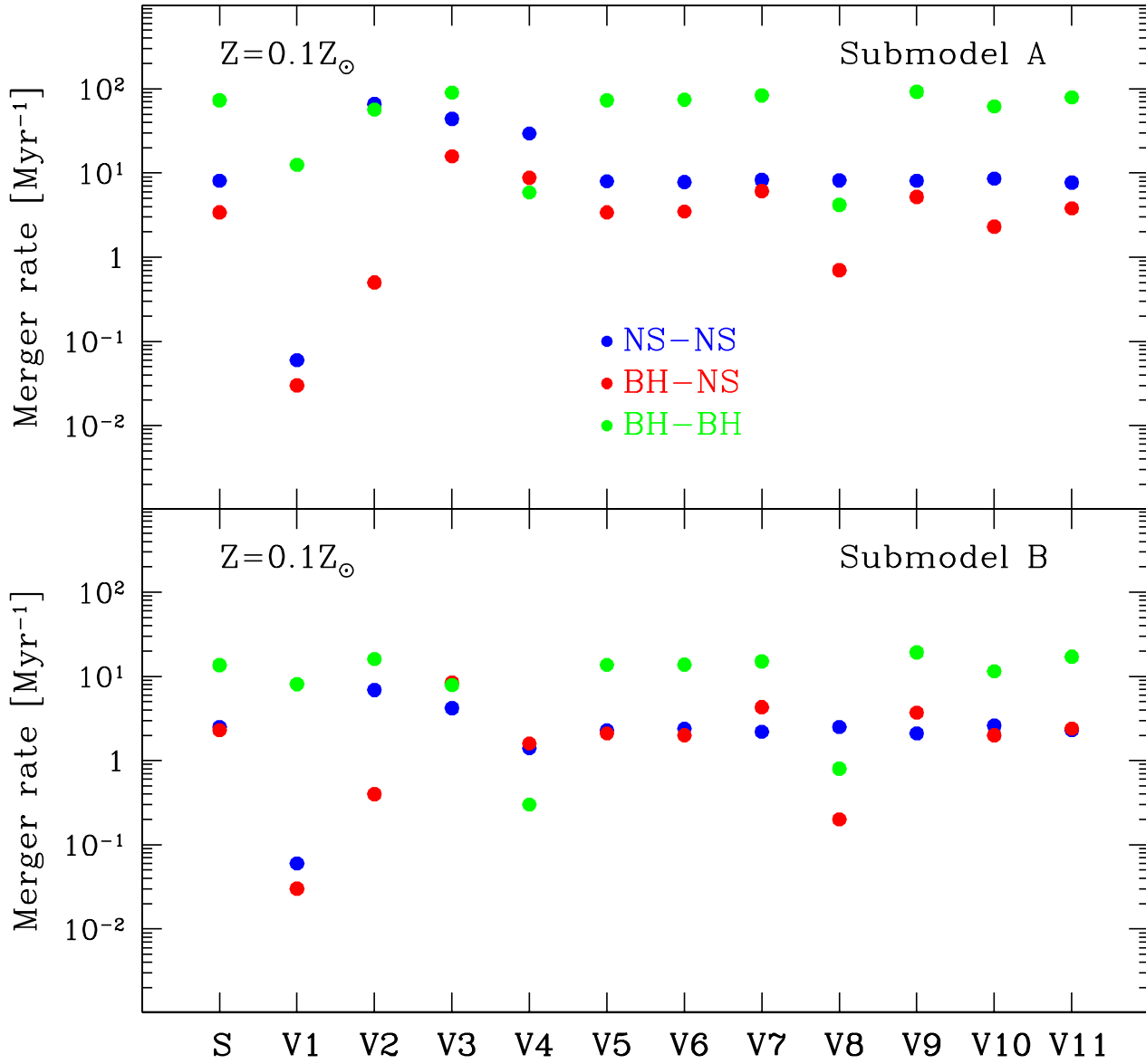


Fig. 20.— Same as Fig. 19 but for $Z = 0.1 Z_{\odot}$.